2-D Analytical Investigation of the Parameters and the Effects of Magnetization Patterns on the Performance of Coaxial Magnetic Gears

A. Rahideh, A. A. Vahaj, M. Mardaneh, T. Lubin

2-D Analytical Investigation of the Parameters and the Effects of Magnetization Patterns on the Performance of Coaxial Magnetic Gears

A. Rahideh [*1], A.A. Vahaj [2], M. Mardaneh [3], T. Lubin[4]

[1] Department of Electrical and Electronics Engineering, Shiraz University of Technology, Shiraz 13876-71557, I.R.Iran
[2] Department of Electrical and Electronics Engineering, Shiraz University of Technology, Shiraz 13876-71557, I.R.Iran
[3] Department of Electrical and Electronics Engineering, Shiraz University of Technology, Shiraz 13876-71557, I.R.Iran
[4]Groupe de Recherche en Electrotechnique et Electronique de Nancy, University of Lorraine, 54506 Nancy, France
[*] A. Rahideh (email: rahide@sutech.ac.ir).

Abstract: In this Paper, a 2-D analytical model has been presented for coaxial magnetic gears. Based on Maxwell's equations the extracted model has been obtained via the solution of the Laplace and Poisson equations by using the separation of variable technique for each sub-region (internal and external magnets, internal and external air-gap and slots). Then the integral coefficients of the general solutions have been obtained by using the boundary conditions and continuity between sub-regions. The proposed analytical model can be used as a tool for design and optimization of magnetic gears. The influences of the number of pole-pair, the magnetization pattern, the size of slot-opening and the segment ratio of the two-segment Halbach pattern on the transmitted torque and unbalanced magnetic forces (UMFs) have been analytically investigated. Finally, to illustrate the efficacy of the proposed model, the analytical results of the magnetic field distribution, transmitted torque and unbalanced magnetic force have been compared with those obtained from finite element analyses.

1. Introduction

Gears are normally used to change the level of torque and speed and can be described as the mechanical counterpart of electrical transformers in which the levels of current and voltage are changed. The first gears had been made out of wood and during the industrial evolutionary cast iron and steel gears were invented. Although mechanical gears have high torque transmission capability and relatively low price, they suffer from several disadvantages such as corrosion, continuous maintenance and lubrication, acoustic noise, heat losses, low efficiency and probability of cog breakage in overload conditions. Therefore, in those applications in which the mentioned issues are not tolerable, an alternative option is a prerequisite. Magnetic gears have several advantages such as no corrosion, low maintenance, lubrication free, low heat losses, high efficiency, high torque density, high reliability, inherent overload protection and capability to combine with brushless permanent magnet (PM) motors to offer pseudo direct drive for many applications such as transmission and power generation [1-3]. Initial magnetic gears were inspired from the mechanical gears and were unsuccessful because of weak magnetic flux density and improper utilization of PMs [4-7]; therefore, the initial concept of magnetic gears could not receive much attention both in academia and

industry. In 2001 by using NdFeB PMs and introducing a novel topology, the concept of magnetic gears has shined again and could provide the transmitted torque density beyond 100 kNm/m^3. Also with the investigation of the magnetic flux density spectrum, the transmitted torque can be maximized with the proper selection of the number of inner and outer pole-pairs and the number of ferromagnetic pole-pieces [8]. In 2004 the influences of the design parameters on the transmitted torque and the torque ripple of magnetic gears have been investigated via numerical approaches [9]. In 2005 the transmitted torque of a coaxial magnetic gear has been calculated by using the finite element method and the results have been compared with those of a prototype [10]. A 2-D analytical model of coaxial magnetic gears has been proposed in 2010 and the model can be used as a tool for optimal design of coaxial magnetic gears [11]. In 2010 another analytical model of magnetic gears with Halbach array for PMs has been presented to calculate the transmitted torque and the torque ripple [12]. A new concept of magnetic gear boxes, which use contra-rotating shaft, has been proposed based on coaxial magnetic gears [13]. A 2-D analytical model of magnetic gears having PMs with the Halbach magnetization pattern has been employed to investigate the influences of the width and height of the pole-pieces and the radial thickness of the outer rotor yoke on the transmitted torque [14]. In [15] a new type of magnetic gear with variable ratio that uses non-rare-earth magnets has been proposed for the applications of hybrid electric vehicles. It is worth noting that 2-D analytical models for different types of PM brushless machines, such as slotless [16]-[18] and slotted [19]-[21] stator structures with different magnetization patterns and multi-segment magnetization pattern [22], inner [16]-[20] and outer [21] rotor topology and surface mounted [16]-[17], [21] surface inset [18]-[19] and consequent-pole [20] have been presented.

In this Paper, a 2-D analytical model for coaxial magnetic gears is presented by solving the governing partial differential equations which are based on the Maxwell equations using the separation of variables technique. The proposed analytical model is presented to be numerically convenient and can incorporate very high harmonic orders and has less computational burden compared to previously reported analytical method. The effects of four different magnetization patterns, i.e. radial, parallel, ideal Halbach and two-segment Halbach, have been investigated on the performance of coaxial magnetic gears in terms of the magnetic flux density distribution, the transmitted torque and the unbalanced magnetic forces (UMFs). Also the influences of the slot-opening ratio and the ratio segment of the two-segment magnetization pattern have been investigated.

This Paper is organized as follows: in Section 2 the basic concept of coaxial magnetic gears is presented. The assumptions and the 2-D analytical model with different magnetization patterns are presented in Section 3. The results of the 2-D analytical model for each magnetization pattern are presented and

compared with those of the finite element method in Section 4. Finally, the concluding remarks are given in Section 5.

2. Basic Concept of Coaxial Magnetic Gears

Fig. 1 shows the illustrative representation of a coaxial magnetic gear. The number of inner rotor pole-pairs, the number of outer rotor pole-pairs and the number of ferromagnetic pole-pieces should obey the following relation to obtain the maximum transmitted torque [9]:

$$P_i + P_o = Q \tag{1}$$

where P_i and P_o are the number of inner and outer rotor pole-pairs respectively and Q is the number of ferromagnetic pole-pieces. The operation of coaxial magnetic gear is based on the modulation of the produced magnetic flux density by each rotor, i.e. the magnetic flux density distributions of the inner and outer rotors are modulated by the ferromagnetic pole-pieces. The modulated flux density has different number of pole-pairs, different magnitude and different rotational speed compared to those of the unmodulated flux density. Assume the number of inner rotor pole-pairs and the number of ferromagnetic pole-pieces are known, the number of outer rotor pole-pairs should be selected to maximally engage with the modulated magnetic flux density of the inner rotor. The gear ratio is defined as the number of driven pole-pairs over the number of the drive pole-pairs.

3. Assumptions and 2-D Analytical Model

As evident from Fig. 1, R_{im} is the inner radius of the inner magnets, R_{ia} is the inner radius of the inner air-gap, R_{is} is the inner radius of the ferromagnetic pole-piece ring, R_{os} is the outer radius of the ferromagnetic pole-piece ring, R_{oa} is the outer radius of the outer air-gap and R_{om} is the outer radius of the

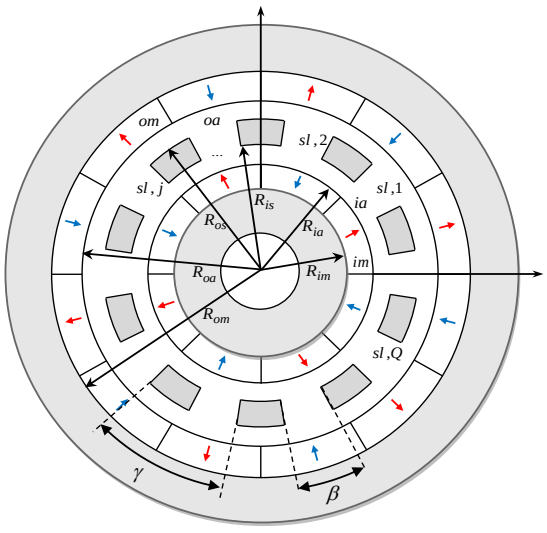

Fig. 1. *Illustrative representation of a coaxial magnetic gear.*

outer magnets. The angular span of each slot is β and the positional angle of each slot edge is obtained as follows:

$$\theta_j = -\beta/2 + 2j\pi/Q + \theta_0 \qquad (2)$$

where j=1, 2, ..., Q and θ_0 is the initial position of the pole-piece ring

3.1. Assumptions

The following assumptions are made to either enable or simplify the analytical model of the magnetic gears:

- The permeability of the back-iron and the ferromagnetic pole-pieces is infinite.
- Relative permeability of PMs is one.
- End effect is neglected.
- Eddy current effects are also neglected.
- In 2-D electromagnetic problems in cylindrical coordinates, the magnetic vector potential has only the axial component which is a function of r and θ.

3.2. 2-D analytical model

Maxwell's equations for magneto-quasi-static approximation are expressed as follows:

Gauss's law for magnetism:

$$\nabla \cdot \mathbf{B} = 0 \qquad (3)$$

Maxwell Faraday equ

ation (Faraday's law of induction):

$$\nabla \times \mathbf{E} = -\frac{\partial \mathbf{B}}{\partial t} \qquad (4)$$

Ampere's circuital law without external current:

$$\nabla \times \mathbf{H} = \mathbf{J} \qquad (5)$$

where **B** is the magnetic flux density vector, **H** is the magnetic field intensity vector, **E** is the electric field vector, and $\mathbf{J}$ is the current density vector in the medium.

The relation between the current density, the electric field and the moving magnetic flux density in a linear isotropic medium can be expressed by

$$\mathbf{J} = \sigma(\mathbf{E} + \mathbf{v} \times \mathbf{B}) \qquad (6)$$

where **v** is the relative velocity vector between the medium and the magnetic field source and σ is the conductivity of the medium.

For a linear medium with magnetization, the relation between **B** and **H** is as follows:

$$\mathbf{B} = \mu_0 \mu_r \mathbf{H} + \mu_0 \mathbf{M} \qquad (7)$$

where **M** is the magnetization vector of the medium which is zero in non-permanent magnet regions and μ_0 and μ_r are the permeability of vacuum and the relative permeability of the medium.

Substituting (7) in Ampere's law, (5), yields:

$$\nabla \times \mathbf{B} = \mu_0 \mu_r \sigma(\mathbf{E} + \mathbf{v} \times \mathbf{B}) + \mu_0 \nabla \times \mathbf{M} \qquad (8)$$

Since **B** is divergence free, i.e. $\nabla \cdot \mathbf{B} = 0$, it can be written in terms of the vector magnetic potential, **A**, as

$$\mathbf{B} = \nabla \times \mathbf{A} \qquad (9)$$

combining (9) and Faraday's law, (4), results in:

$$\nabla \times \mathbf{E} = -\frac{\partial(\nabla \times \mathbf{A})}{\partial t} \rightarrow \mathbf{E} = -\frac{\partial \mathbf{A}}{\partial t} - \nabla V \qquad (10)$$

where V is the electric scalar potential.

Combining (8), (9) and (10) yields:

$$-\nabla^2 \mathbf{A} + \mu_0 \mu_r \sigma \left(\frac{\partial \mathbf{A}}{\partial t} + \nabla V - \mathbf{v} \times \nabla \times \mathbf{A} \right) = \mu_0 \nabla \times \mathbf{M} \qquad (11)$$

In 2-D polar coordinates, some of the components of the vectors are zero:

$$\begin{aligned} \mathbf{A} &= \left[0, 0, A_z(r, \theta)\right] \\ \mathbf{M} &= \left[M_r(\theta), M_\theta(\theta), 0\right] \\ \mathbf{B} &= \left[B_r(r, \theta), B_\theta(r, \theta), 0\right] \end{aligned} \qquad (12)$$

where A_z is the axial component of the vector magnetic potential, M_r and M_θ are the magnetization vector components in the radial and tangential directions respectively and B_r and B_θ are the flux density vector components in the radial and tangential directions respectively. Therefore, in 2-D polar coordinates, the following expression is obtained:

$$-\frac{1}{r}\frac{\partial}{\partial r}\left(r\frac{\partial A_z^i}{\partial r}\right)-\frac{1}{r^2}\frac{\partial^2 A_z^i}{\partial \theta^2}+\mu_0\mu_r\sigma\left(\frac{\partial A_z^i}{\partial t}+\Omega\frac{\partial A_z^i}{\partial \theta}\right)= \quad (13)$$
$$\frac{\mu_0}{r}\left(\frac{\partial}{\partial r}\left(rM_\theta^i\right)-\frac{\partial M_r^i}{\partial \theta}\right)$$

Assuming the eddy current field is neglected, the following Poisson and Laplace equations are obtained in the PM region and air-gap/slot regions, respectively

$$-\frac{1}{r}\frac{\partial}{\partial r}\left(r\frac{\partial A_z^i}{\partial r}\right)-\frac{1}{r^2}\frac{\partial^2 A_z^i}{\partial \theta^2}=\frac{\mu_0}{r}\left(\frac{\partial}{\partial r}\left(rM_\theta^i\right)-\frac{\partial M_r^i}{\partial \theta}\right) \quad (14)$$

$$-\frac{1}{r}\frac{\partial}{\partial r}\left(r\frac{\partial A_z^i}{\partial r}\right)-\frac{1}{r^2}\frac{\partial^2 A_z^i}{\partial \theta^2}=0 \quad (15)$$

where i= {*im*, *om*} in the PM regions and i= {*ia*, *oa*, *sl*,*j*} in the air-gap/slot regions and *im*, *om*, *ia*, *oa*, *sl*,*j* are respectively the superscripts for inner magnet, outer magnet, inner air-gap, outer air-gap and *j*-th slot. The general solution for each sub-region is found to satisfy the corresponding PDEs and also has the ability to satisfy the boundary/interface conditions. The boundary/interface conditions are as follows:

$$A_z^i = A_z^{i+} \quad (16)$$

$$H_\theta^i = H_\theta^{i+} \quad (17)$$

where i and i+ are the indices of two adjacent regions.

The relation between the non-zero components of **B** and **A** in polar coordinates is as follows:

$$B_\theta^i(r,\theta)=-\frac{\partial A_z^i}{\partial r} \quad (18)$$

$$B_r^i(r,\theta)=\frac{1}{r}\frac{\partial A_z^i}{\partial \theta} \quad (19)$$

Based on expressions (16) and (17), the boundary conditions between each pair of adjacent sub-regions are tabulated in Table 1:

Table 1 boundary and interface conditions

Region i	Region i+	Boundary/interface conditions	Interface	Applied range	
Inner PMs	Inner back-iron	$H_\theta^{im}(r,\theta)=0$	$r=R_{im}$	$-\pi<\theta<\pi$	(20)
		$A_z^{im}(r,\theta)=A_z^{ia}(r,\theta)$	$r=R_{ia}$	$-\pi<\theta<\pi$	(21)

	Inner air-gap	$H_\theta^{im}(r,\theta)=H_\theta^{ia}(r,\theta)$			(22)
Inner air-gap	Slot j	$A_z^{ia}(r,\theta)=A_z^{sl,j}(r,\theta)$	$r=R_{is}$	$\theta_j<\theta<\theta_j+\beta$ $j=1,2,...,Q$	(23)
	slots	$H_\theta^{ia}(r,\theta)=\sum_{j=1}^{Q}H_\theta^{sl,j}(r,\theta)$			(24)
Outer air-gap	Slot j	$A_z^{sl,j}(r,\theta)=A_z^{oa}(r,\theta)$	$r=R_{os}$	$\theta_j<\theta<\theta_j+\beta$ $j=1,2,...,Q$	(25)
	Slots	$\sum_{j=1}^{Q}H_\theta^{sl,j}(r,\theta)=H_\theta^{oa}(r,\theta)$			(26)
Outer PMs	Outer air-gap	$A_z^{oa}(r,\theta)=A_z^{om}(r,\theta)$	$r=R_{oa}$	$-\pi<\theta<\pi$	(27)
		$H_\theta^{oa}(r,\theta)=H_\theta^{om}(r,\theta)$			(28)
	Outer back-iron	$H_\theta^{om}(r,\theta)=0$	$r=R_{om}$	$-\pi<\theta<\pi$	(29)

And according to [11]

$$\int_0^{2\pi}H_\theta^{im}\Big|_{r=R_{ia}}d\theta=\int_0^{2\pi}\sum_{j=1}^{Q}H_\theta^{sl,j}\Big|_{r=R_{is}}d\theta \tag{30}$$

The combined general and particular solutions for the inner and outer magnet regions are as follows:

$$\begin{aligned}A_z^i(r,\theta)=&\sum_{n=1}^{\infty}\left[a_n^i r^n+b_n^i r^{-n}\right]\cos(n\theta)+\\&\sum_{n=1}^{\infty}\left[c_n^i r^n+d_n^i r^{-n}\right]\sin(n\theta)+A_{z_p}^i\end{aligned} \tag{31}$$

where the particular solution is as follows:

$$A_{z_p}^i=\sum_{n=1}^{\infty}\left[K_{n1}^i(r)\cos(\mathrm{n}\theta)+K_{n2}^i(r)\sin(\mathrm{n}\theta)\right] \tag{32}$$

where i={*im*, *om*} and n is a positive integer value and a_n^i, b_n^i, c_n^i and d_n^i are the integral coefficients to be determined by applying the boundary/interface conditions. $K_{n1}(r)$ and $K_{n2}(r)$ are the particular solutions which depend on the magnetization patterns.

The general solutions in the inner and outer air-gap regions are as follows:

$$A_z^i(r,\theta) = a_0^i + \sum_{n=1}^{\infty}\left[a_n^i r^n + b_n^i r^{-n}\right]\cos(n\theta) + \sum_{n=1}^{\infty}\left[c_n^i r^n + d_n^i r^{-n}\right]\sin(n\theta) \quad (33)$$

where i={ia,, oa}, n is a positive integer value and a_0^i, a_n^i, b_n^i, c_n^i and d_n^i are the integral coefficients to be found.

The general solutions in the slot regions are expressed as:

$$\mathrm{A}_z^{sl,j}(r,\theta) = a_0^{sl,j} + b_0^{sl,j}\ln(r) + \sum_{u=1}^{\infty}\left[a_u^{sl,j} r^{u\pi/\beta} + b_u^{sl,j} r^{-u\pi/\beta}\right]\cos\left(\frac{u\pi}{\beta}(\theta-\theta_j)\right) \quad (34)$$

where j=1, 2, ..., Q, Q is the number of slots, u is a positive integer value and $a_0^{sl,j}$, $b_0^{sl,j}$, $a_u^{sl,j}$ and $b_u^{sl,j}$ are the integral coefficients to be obtained. For the sake of convenience in the numerical calculations, the solutions are rewritten as follows:

$$A_z^i(r,\theta) = \sum_{n=1}^{\infty}\left[\hat{a}_n^i\left(\frac{r}{R_{i+}}\right)^n + \hat{b}_n^i\left(\frac{R_{i-}}{r}\right)^{-n} + K_{n1}^i(r)\right]\cos(n\theta) + \sum_{n=1}^{\infty}\left[\hat{c}_n^i\left(\frac{r}{R_{i+}}\right)^n + \hat{d}_n^i\left(\frac{R_{i-}}{r}\right)^{-n} + K_{n2}^i(r)\right]\sin(n\theta) \quad (35)$$

where $(i, R_{i+}, R_{i-}) = \{(im, R_{ia}, R_{im}), (om, R_{om}, R_{oa})\}$

$$A_z^i(r,\theta) = a_0^i + \sum_{n=1}^{\infty}\left[\hat{a}_n^i\left(\frac{r}{R_{i+}}\right)^n + \hat{b}_n^i\left(\frac{R_{i-}}{r}\right)^{-n}\right]\cos(n\theta) + \sum_{n=1}^{\infty}\left[\hat{c}_n^i\left(\frac{r}{R_{i+}}\right)^n + \hat{d}_n^i\left(\frac{R_{i-}}{r}\right)^{-n}\right]\sin(n\theta) \quad (36)$$

where $(i, R_{i+}, R_{i-}) = \{(ia, R_{is}, R_{ia}), (oa, R_{oa}, R_{os})\}$

$$A_z^{sl,j}(r,\theta) = a_0^{sl,j} + b_0^{sl,j}\ ln(r)\ + \sum_{u=1}^{\infty}\left[\hat{a}_u^{sl,j}\left(\frac{r}{R_{os}}\right)^{u\pi/\beta} + \hat{b}_u^{sl,j}\left(\frac{R_{is}}{r}\right)^{-u\pi/\beta}\right]\cos\left(\frac{u\pi}{\beta}(\theta-\theta_j)\right) \qquad (37)$$

The boundary/interface conditions (20) -(30) are imposed to the general solutions to obtain the integral coefficients. By imposing the boundary/interface conditions, a set of algebraic simultaneous equations, in which the integral coefficients are unknown, is formed as listed in the Appendix.

Up to here, the common procedure of the 2-D analytical modelling technique, regardless of the magnetization pattern, has been presented. The next step is to determine $K_{n1}^{i}(r)$ and $K_{n2}^{i}(r)$ for each of the magnetization patterns, i.e. radial, parallel, ideal Halbach and 2-segment Halbach. To this end, the particular solution, (32), and the Fourier series expansions of M_r^i and M_θ^i for each magnetization pattern are substituted in (14) and these yields $K_{n1}^{i}(r)$ and $K_{n2}^{i}(r)$ in terms of the Fourier series expansion components of M_r^i and M_θ^i.

Four different magnetization patterns along with their radial and tangential components are shown in Fig. 2 for inner and outer magnets and their expression are listed in the Appendix. Based on (20) -(30), the number of algebraic equations and unknown integral coefficients are (2+2U) Q+16N+1 for each magnetization pattern, where U is the maximum number of harmonics in the slot region and N is the maximum number of harmonics in the other regions. The algebraic simultaneous equations are solved for each magnetization patterns to obtain the integral coefficients.

3.3. Flux density distribution

The radial and tangential components of the magnetic flux density vector in the inner and outer air-gaps are calculated by substituting the magnetic vector potential in (18) and (19):

$$B_r^{ia}(r,\theta) = \sum_{n=1}^{N}\left(\hat{a}_n^{ia}\frac{-n}{r}\left(\frac{r}{R_{is}}\right)^{n} + \hat{b}_n^{ia}\frac{-n}{r}\left(\frac{r}{R_{ia}}\right)^{-n}\right)\sin(n\theta) + \sum_{n=1}^{N}\left(\hat{c}_n^{ia}\frac{n}{r}\left(\frac{r}{R_{is}}\right)^{n} + \hat{d}_n^{ia}\frac{n}{r}\left(\frac{r}{R_{ia}}\right)^{-n}\right)\cos(n\theta) \qquad (38)$$

$$B_\theta^{ia}(r,\theta)=\sum_{n=1}^{N}\left(\hat{a}_n^{ia}\frac{-n}{r}\left(\frac{r}{R_{is}}\right)^{n}+\hat{b}_n^{ia}\frac{n}{r}\left(\frac{r}{R_{ia}}\right)^{-n}\right)\cos(n\theta)$$
$$+\sum_{n=1}^{N}\left(\hat{c}_n^{ia}\frac{-n}{r}\left(\frac{r}{R_{is}}\right)^{n}+\hat{d}_n^{ia}\frac{n}{r}\left(\frac{r}{R_{ia}}\right)^{-n}\right)\sin(n\theta) \qquad (39)$$

where B_r^{ia} , B_θ^{ia} are the radial and tangential components of the magnetic flux density vector in the inner air-gap.

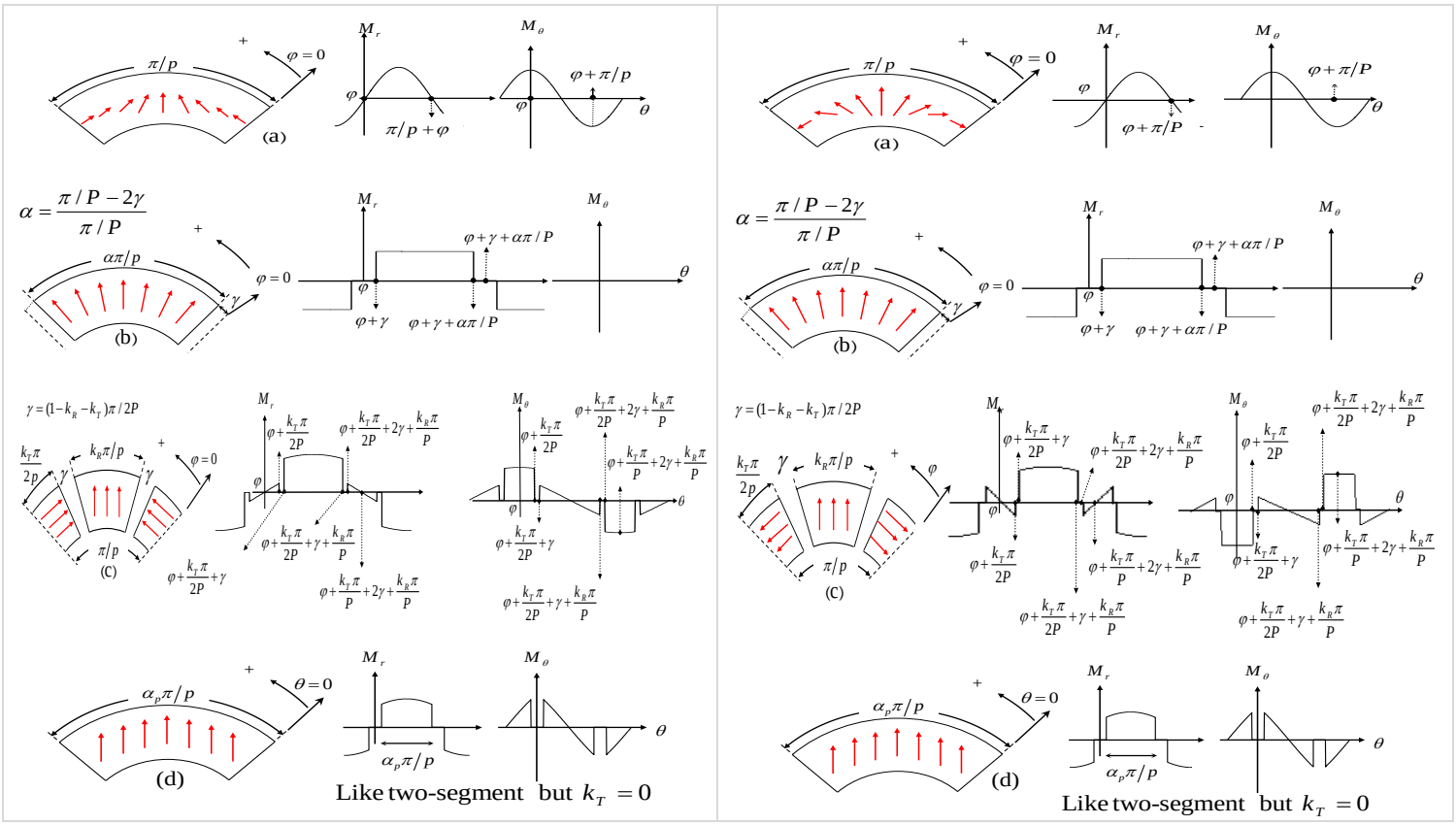

Fig. 2. *Four different Magnetization patterns along with the radial and tangential components*
I. for inner rotor (a) ideal Halbach; (b) radial; (c) two-segment Halbach; (d) parallel
II. for outer rotor (a) ideal Halbach; (b) radial; (c) two-segment Halbach; (d) parallel

$$B_r^{oa}(r,\theta)=\sum_{n=1}^{N}\left(\hat{a}_n^{oa}\frac{-n}{r}\left(\frac{r}{R_{oa}}\right)^{n}+\hat{b}_n^{oa}\frac{-n}{r}\left(\frac{r}{R_{os}}\right)^{-n}\right)\sin(n\theta)$$
$$+\sum_{n=1}^{N}\left(\hat{c}_n^{oa}\frac{n}{r}\left(\frac{r}{R_{oa}}\right)^{n}+\hat{d}_n^{oa}\frac{n}{r}\left(\frac{r}{R_{os}}\right)^{-n}\right)\cos(n\theta) \qquad (40)$$

$$B_\theta^{oa}(r,\theta)=\sum_{n=1}^{N}\left(\hat{a}_n^{oa}\frac{-n}{r}\left(\frac{r}{R_{oa}}\right)^n+\hat{b}_n^{oa}\frac{n}{r}\left(\frac{r}{R_{os}}\right)^{-n}\right)\cos(n\theta)$$
$$+\sum_{n=1}^{N}\left(\hat{c}_n^{oa}\frac{-n}{r}\left(\frac{r}{R_{oa}}\right)^n+\hat{d}_n^{oa}\frac{n}{r}\left(\frac{r}{R_{os}}\right)^{-n}\right)\sin(n\theta) \qquad (41)$$

where B_r^{oa} , B_θ^{oa} are the radial and tangential components of the magnetic flux density vector in the outer air-gap.

3.4. Transmitted torque

The transmitted torque of magnetic gears is one of the most important quantities in order to investigate the capability of the system. Having calculated the radial and tangential components of the magnetic flux density in the inner and outer air-gap, equations (38) -(41), the torque of the inner and outer rotors is computed by using the Maxwell stress tensor, along a specific line or contour as follows [23]:

$$\mathbf{F}=\iint\left[\frac{1}{\mu_0}\mathbf{B}\left(\mathbf{B}\cdot\mathbf{n}\right)-\frac{1}{2\mu_0}\mathbf{B}^2\mathbf{n}\right]dS \qquad (42)$$

Therefore, normal and tangential forces on the body surrounded by surface S are obtained as:

$$F_n=\frac{L}{\mu_0}\int\left[B_n^2-B_t^2\right]dl \quad (43) \qquad F_t=\frac{L}{\mu_0}\int\left[B_nB_t\right]dl \quad (44)$$

where B_n and B_t are the normal and tangential components of the magnetic flux density. L is the axial length of surface S. In polar 2-D problems, they are expressed as follow:

$$F_r=\frac{L}{\mu_0}\int\left[B_r^2-B_\theta^2\right]d\theta \qquad (45), \qquad F_\theta=\frac{Lr}{\mu_0}\int\left[B_rB_\theta\right]d\theta \qquad (46)$$

The torque is obtained using $\mathbf{T}=\mathbf{r}\times\mathbf{F}$ which results in the following expression:

$$F_\theta=\frac{Lr^2}{\mu_0}\int\left[B_rB_\theta\right]d\theta \qquad (47)$$

Therefore, the inner and outer rotor torque relations are respectively represented in (48) and (49)

$$T_{in}=\frac{LR_{m1}^2}{\mu_0}\int_0^{2\pi}B_r^{ia}(R_{m1},\theta).B_\theta^{ia}(R_{m1},\theta).d\theta \qquad (48)$$

$$T_{out}=\frac{LR_{m2}^2}{\mu_0}\int_0^{2\pi}B_r^{oa}(R_{m2},\theta).B_\theta^{oa}(R_{m2},\theta).d\theta \qquad (49)$$

where L is the axial length of magnetic gear and R_{m1} and R_{m2} are the average radii of the inner and outer air-gap respectively defined as $\mathrm{R}_{m_1}=(R_{ia}+R_{is})/2, \mathrm{R}_{m_2}=(R_{os}+R_{oa})/2$

3.5. Unbalanced magnetic force

Another important quantity in magnetic gears is the unbalanced magnetic force, which imposes undesirable radial forces to the system and reduces the bearing lifetime. Based on the Maxwell stress tensor, the radial and tangential components of the magnetic local traction acting on each rotor surface can be obtained as:

$$f_r = \frac{1}{2\mu_0}\left(B_r^2 - B_\theta^2\right) \qquad (50)$$

$$f_\theta = \frac{1}{\mu_0} B_r B_\theta \qquad (51)$$

Transforming these equations to the Cartesian coordinates yields:

$$f_x = f_r \cos(\theta) - f_\theta \sin(\theta) \qquad (52)$$

$$f_y = f_r \sin(\theta) + f_\theta \cos(\theta) \qquad (53)$$

The components of the magnetic unbalanced force exerted on each rotor center are calculated over a circular surface of radius *r* normally in the middle of each air gap as

$$F_x(t) = L \int_{-\pi}^{\pi} f_x r d\theta \qquad (54)$$

$$F_y(t) = L \int_{-\pi}^{\pi} f_y r d\theta \qquad (55)$$

$$|F| = \sqrt{F_x^2(t) + F_y^2(t)} \qquad (56)$$

4. Results

To evaluate the performance of the 2-D analytical model, three case studies, each with four magnetization patterns, with the parameters listed in Table 2 have been employed. The specifications of the three case studies are almost similar and the difference is due to the number of inner and outer pole-pairs. The effects of slot-opening ratio ($\beta' = \beta / \gamma$) on the performance of the three magnetic gears have also been investigated. Besides, the influence of the segment ratio (K_R) on the transmitted torque and torque ripple of the three magnetic gears have been examined in the case of 2-segment magnetization pattern. As mentioned in Table 2, the maximum number of harmonics for each region is set to 100; however due to the numerically convenient form of the presented expressions, the maximum number of harmonics in each region is theoretically unlimited and the limitation is affected by the computer specifications to handle the

computational burden. Obviously the proper value for the maximum number of harmonics is obtained with a compromise between the required accuracy and the computational burden.

4.1. Flux density distribution

The radial and tangential components of the magnetic flux density for case 1 in the middle of the inner and outer air-gaps are shown in Fig. 3 for the different magnetization patterns, i.e., two-segments Halbach, radial, ideal Halbach and parallel. The finite element method has been used to investigate the efficacy of the proposed analytical mode. For the investigation of the analytical magnetic flux density calculation, the magneto-static simulation has been used and for the investigation of the analytical torque and UMF calculations, the transient simulation has been employed in which the rotational velocity of the high speed rotor is set to 1000 rpm, and the step time is set to 0.006 seconds. The comparative study shows a good agreement between the numerical and analytical results.

It is noted that the slot-opening ratio is assumed to be 0.5 in Fig. 3 and the segment ratio is set to 0.5 for the two-segment magnetization pattern and the positions of inner and outer rotors are set to zero.

Table 2 Parameters of the Case Studies

Parameters	symbols	Case 1	Case 2	Case 3
Inner radius of inner PMs	R_{im}		4cm	
Inner radius of inner air-gap	R_{ia}		5cm	
Inner radius of slots	R_{is}		5.2cm	
Outer radius of slots	R_{os}		6.2cm	
Outer radius of outer air-gap	R_{oa}		6.4cm	
Outer radius of outer PMs	R_{om}		7.4cm	
Axial length	L		10cm	
Remenance of PMs	B_r		1.2T	
Number of inner rotor pole-pairs	P_i	2	2	4
Number of outer rotor pole-pairs	P_o	3	21	22
Number of ferromagnetic pole-pieces	Q	5	23	26
Maximum number of harmonics in the air- gap and PMs regions	N		100	
Maximum number of harmonics in the slots	U		100	

4.2. Torque

The pull-out torque waveforms of the coaxial magnetic gears with different magnetization patterns for the three case studies are depicted in Fig. 4 in which the outer rotor and the pole-pieces are kept stationary. As evident from the figures, the maximum torque is obtained when the initial position of the inner rotor for

all magnetization patterns is set to 45° for case 1 (P_i=2, P_o=3) and case 2 (P_i=2, P_o =21) and is set to 22.5 ° for case 3 (P_i =4, P_o =22).

Fig. 5 show the torque of the inner and outer rotors for the three cases with different magnetization patterns where the pole-pieces are kept stationary and the inner and outer rotors are rotated according to the following expression:

$$\frac{T_i}{T_o} = \frac{\omega_o}{\omega_i} = -\frac{P_i}{P_o} \qquad (57)$$

Based on the principle of coaxial magnetic gears, the inner and outer rotors rotate in the opposite directions and the ratio of the transmitted torque from the inner rotor to the outer rotor is -P_o/P_i. As mentioned before in all the case studies $\beta' = 0.5$ and for the 2-segment magnetization pattern $K_R = 0.5$.

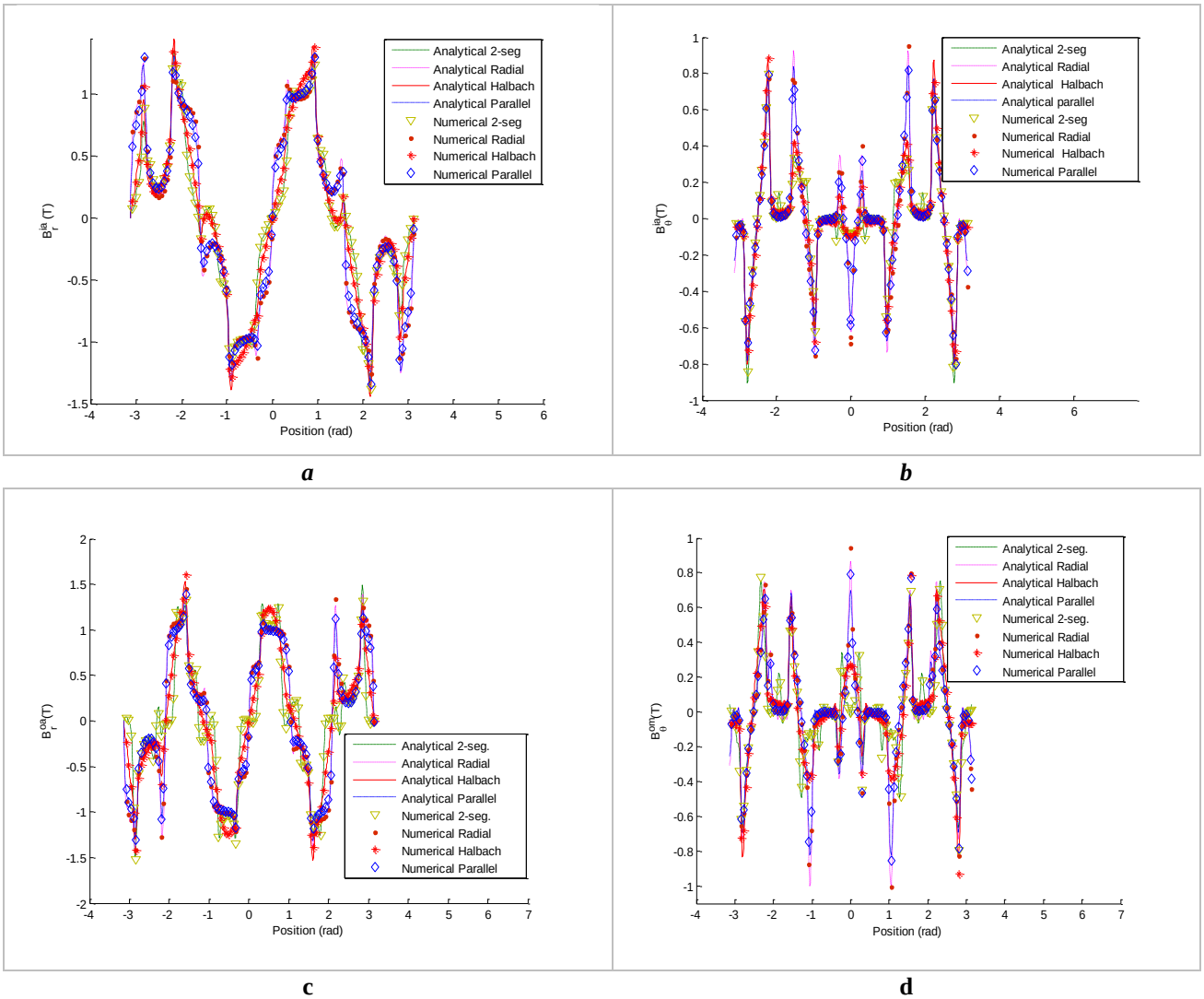

Fig. 3. *Components of the magnetic flux density for case 1 with different magnetization patterns.*
a Radial component of the magnetic flux density in the middle of the inner air-gap
b Tangential component of the magnetic flux density in the middle of the inner air-gap

c Radial component of the magnetic flux density in the middle of the outer air-gap
d Tangential component of the magnetic flux density in the middle of the outer air-gap

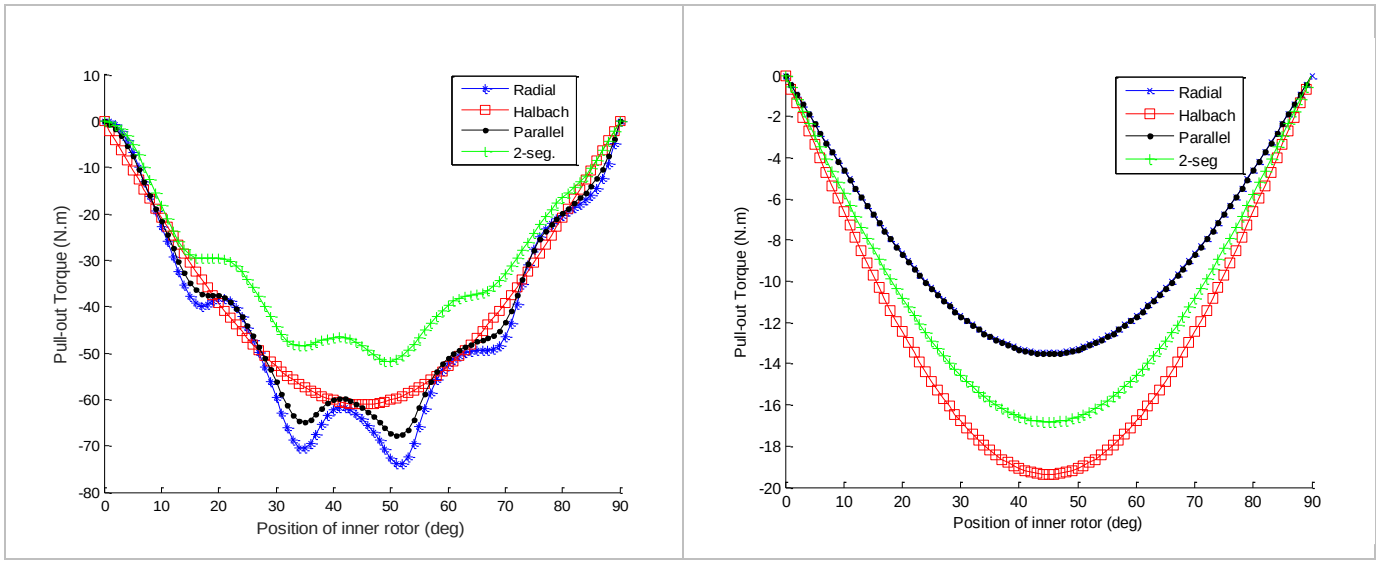

a

b

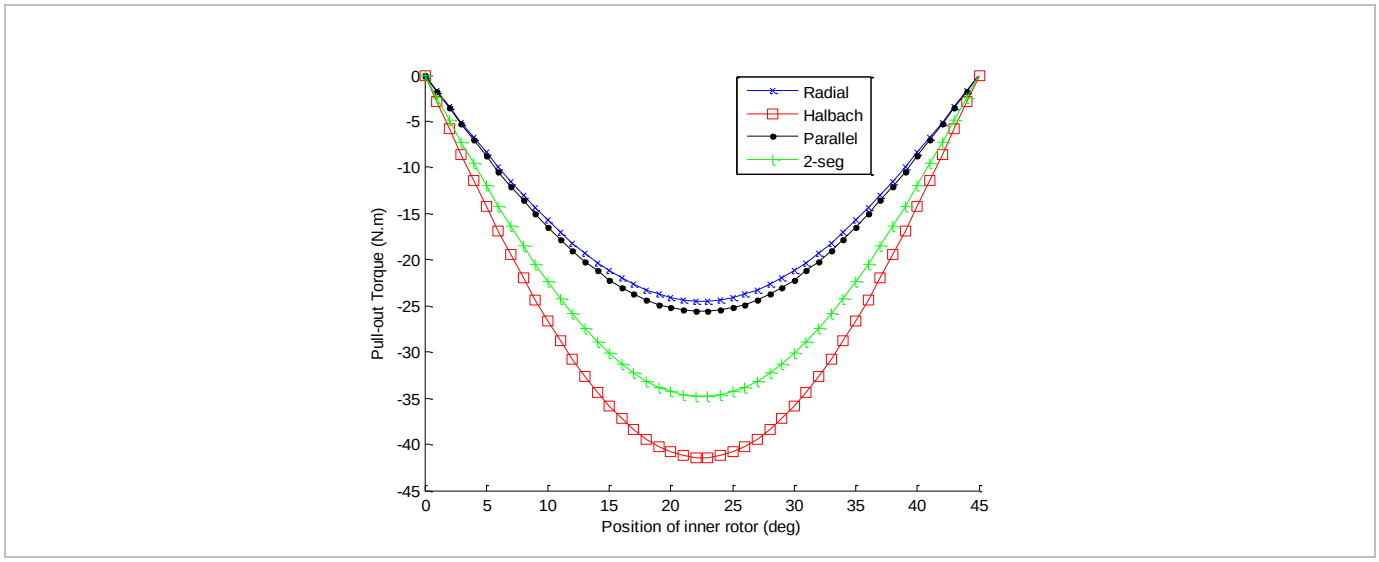

c

Fig. 4 . *Pull-out torque of the inner rotor for all cases with different magnetization patterns*

a Case 1 where the outer rotor is kept stationary and the inner rotor is rotated from 0 to 90 degrees.
b Case 2 where the outer rotor is kept stationary and the inner rotor is rotated from 0 to 90 degrees.
c Case 3 where the outer rotor is kept stationary and the inner rotor is rotated from 0 to 45 degrees.

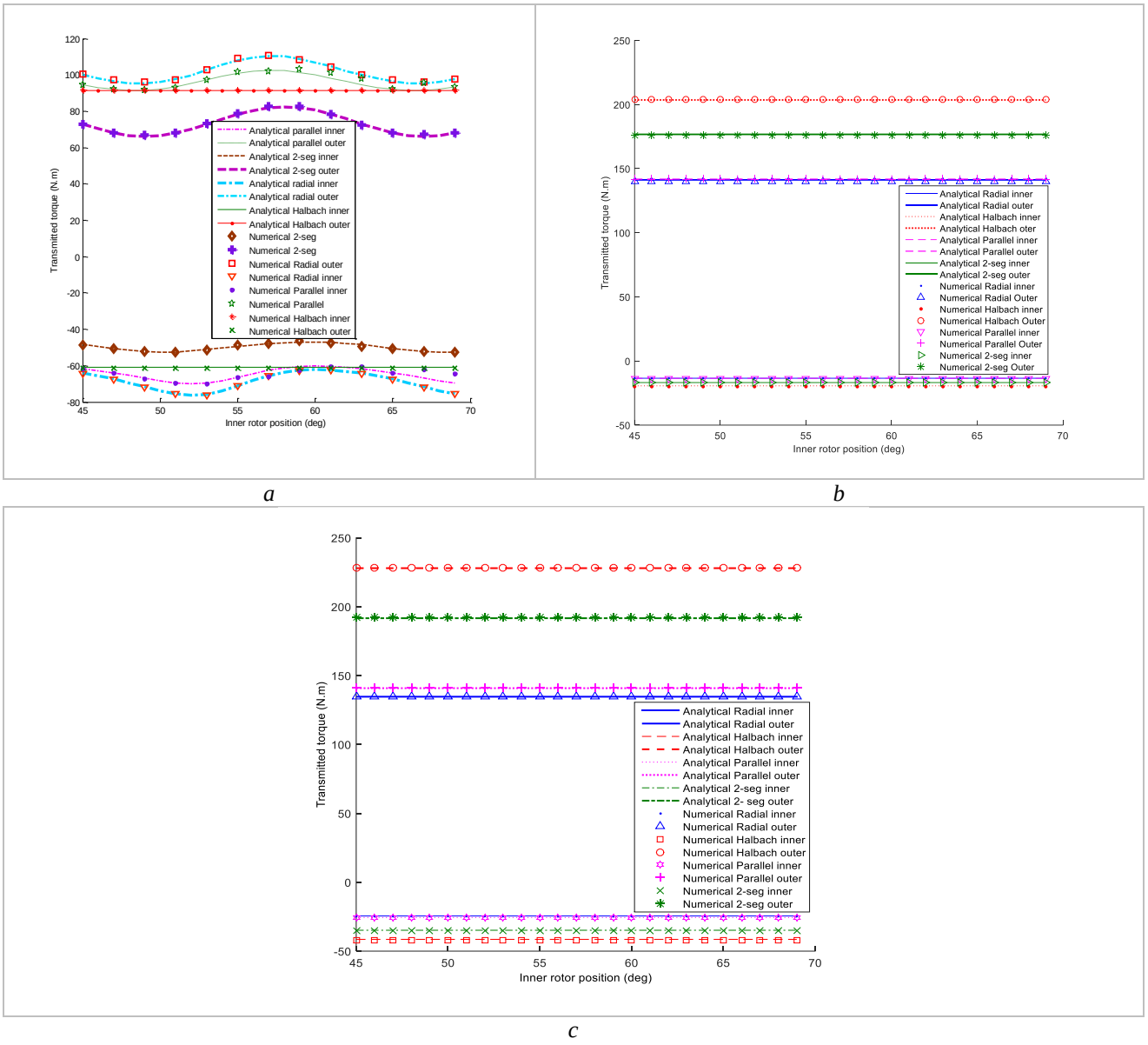

Fig. 5. *Transmitted torque of the inner and outer rotors for all cases with different magnetization patterns.*

a Case1
b Case2
c Case3

As evident from Fig. 5.a in case 1 the best performance in terms of the torque average is obtained by the radial magnetization pattern and followed by parallel, ideal Halbach and 2-segment Halbach magnetization patterns respectively. In case 1, the Halbach magnetization pattern has the minimum torque ripple in comparison to other magnetization patterns. Fig. 5. b. which is related to case 2 (P_i =2 and P_o=21), shows completely different results compared to case 1 (P_i =2 and P_o=3). As illustrated in Fig. 5.b the highest transmitted torque is for the ideal Halbach magnetization pattern, followed by the two-segment Halbach, parallel and radial magnetization patterns respectively. However, the torque ripple is not considerable in all

magnetization patterns. The transmitted torque waveform for case 3, Pi =4 and Po=22, is shown in Fig. 5.c and has similar interpretation as for case 2.

4.3. Effects of slot-opening ratio

In order to investigate the influence of the slot-opening ratio on the performance of magnetic gears, the slot-opening ratio is changed and the results are tabulated in Table 3 for the three case studies with radial magnetization pattern. Similar investigations for the magnetic gears with the ideal Halbach and parallel magnetization patterns are conducted and their results are reported in Tables 4 and 5 respectively. Tables 6 and 7 show the results of the variation of the slot-opening ratio for the magnetic gears with the two-segment magnetization pattern having segment ratio of 0.5 and 0.8 respectively. When the number of pole-pieces is low, the peak of the transmitted torque occurs at low slot-opening ratio, i.e. $\beta' = 0.25$. However, as the number of pole-pieces increases, the maximum torque is transmitted when the slot-opening ratio is set to 0.5. The ratio of torque ripples in the outer and inner rotors of magnetic gears is influenced not only by the gear ratio but also by the slot-opening to slot-pitch ratio.

Table 3 The average torque and torque ripple for three case studies with different slot ratios in radial magnetization pattern.

		Average torque (N.m)		Torque ripple (N.m)	
	β'	Inner	Outer	Inner	Outer
Pi=2 Po=3	0.25	-80.146	119.769	11.796	7.032
	0.3	-81.229	121.447	12.557	8.936
	0.55	-62.404	92.633	12.989	14.184
	0.65	-47.068	70.011	6.828	11.810
Pi=2 Po=21	0.25	-11.329	118.952	0.017	1.393
	0.3	-11.877	124.712	0.008	0
	0.55	-13.598	142.776	0.004	0
	0.65	-13.245	139.076	0.009	0
Pi=4 Po=22	0.25	-19.825	109.037	0	0
	0.30	-21.380	117.591	0	0
	0.55	-24.513	134.824	0	0
	0.65	-23.570	129.637	0	0

Table 4 The average torque and torque ripple for three case studies with different slot ratios in ideal halbach magnetization pattern.

		Average torque (N.m)		Torque ripple (N.m)	
	β'	Inner	Outer	Inner	Outer
P_i=2 P_o=3	0.25	-72.880	109.320	0	0
	0.3	-73.324	109.985	0	0
	0.55	-55.862	83.789	0.002	0.004
	0.65	-44.440	66.661	0	0
P_i=2 P_o=21	0.25	-16.328	171.447	0	0
	0.3	-17.119	179.749	0	0
	0.55	-19.598	205.785	0	0
	0.65	-19.091	200.453	0	0
P_i=4 P_o=22	0.25	-33.559	184.573	0	0
	0.30	-36.191	199.053	0	0
	0.55	-41.495	228.224	0	0
	0.65	-39.899	219.445	0	0

Table 5 The average torque and torque ripple for three case studies with different slot ratios in parallel magnetization pattern.

		Average torque (N.m)		Torque ripple (N.m)	
	β'	Inner	Outer	Inner	Outer
P_i=2 P_o=3	0.25	-76.095	113.882	8.231	5.437
	0.3	-76.969	115.191	9.035	6.677
	0.55	-58.979	87.822	9.167	10.536
	0.65	-45.276	67.459	4.727	8.903
P_i=2 P_o=21	0.25	-11.377	119.460	0.009	0
	0.3	-11.928	125.244	0.005	0
	0.55	-13.656	143.385	0.002	0
	0.65	-13.302	139.670	0.005	0
P_i=4 P_o=22	0.25	-20.737	114.052	0	0
	0.3	-22.363	122.999	0	0
	0.55	-25.641	141.024	0	0
	0.65	-24.654	135.599	0	0

Table 6 The average torque and torque ripple for three case studies with different slot ratios in two-segment magnetization pattern. (K_R=K_T =0.5)

		Average torque (N.m)		Torque ripple (N.m)	
	β'	Inner	Outer	Inner	Outer
P_i=2 P_o=3	0.25	-58.602	87.708	6.257	4.948
	0.3	-58.835	88.305	5.142	13.872
	0.55	-45.104	67.851	4.382	10.404
	0.65	-35.681	53.271	2.909	12.123
P_i=2 P_o=21	0.25	-14.176	148.851	0.006	0
	0.3	-14.863	156.059	0.003	0
	0.55	-17.015	178.663	0.002	0
	0.65	-16.575	174.034	0.004	0
P_i=4 P_o=22	0.25	-28.213	155.171	0	0
	0.3	-30.426	167.344	0	0
	0.55	-34.885	191.868	0	0
	0.65	-33.543	184.487	0	0

Table 7 The average torque and torque ripple for three case studies with different slot ratios in two-segment magnetization pattern. (K_R=0.8, K_T=0.2)

		Average torque (N.m)		Torque ripple (N.m)	
	β'	Inner	Outer	Inner	Outer
P_i=2 P_o=3	0.25	-79.378	118.638	4.1479	11.121
	0.3	-80.474	120.298	5.734	8.170
	0.55	-61.434	91.508	5.918	9.467
	0.65	-47.104	70.278	5.343	7.211
P_i=2 P_o=21	0.25	-14.219	149.302	0.006	0
	0.3	-14.908	156.531	0.003	0
	0.55	-17.067	179.204	0.001	0
	0.65	-16.625	174.561	0.003	0
P_i=4 P_o=22	0.25	-27.236	149.800	0	0
	0.3	-29.373	161.552	0	0
	0.55	-33.678	185.227	0	0
	0.65	-32.382	178.102	0	0

4.4. Effects of segment ratio of 2-segment magnetization pattern

Fig. 6 shows the transmitted torque and torque ripple variation as functions of segment ratio of 2-segment magnetization pattern. As evident, when the number of pole-pieces is low, the higher ratio of the parallel segment compared to that of the tangential segment causes a higher transmitted torque. However, when the number of pole-pieces increases, to obtain the maximum transmitted torque, it is required to relatively decrease the parallel segment ratio. Therefore, in Fig. 6.a which is related to case 1 (P_i=2, P_o=3) the maximum transmitted torque occurs at the segment ratio of 0.8 which also has minimum torque ripple. In Fig. 6.a and b, which respectively illustrates the results of case 2 (P_i=2, P_o=21) and case 3 (P_i=4, P_o=22), the maximum torque is transmitted at the segment ratio of 0.6 where the torque ripple is zero.

4.5. Unbalanced Magnetic Force

Fig. 7.a shows the modulus of the UMF for case 1 (P_i=2, P_o=3) with different magnetization patterns. As evident from the figure, a high amount of UMF is exerted on both rotors. Note that in this case study, the magnetic gear with two-segment magnetization pattern has relatively the lowest UMF compared to that of the other magnetization patterns. The modulus of the UMF for case 2 (P_i=2, P_o=21) is illustrated in Fig. 7.b in which the highest to the lowest UMFs are respectively due to radial, parallel, two-segment Halbach and ideal Halbach magnetization patterns. It is noted that the ideal Halbach magnetization pattern has almost no UMF. The UMF for case 3 (P_i=4, P_o=22) with different magnetization patterns is almost zero.

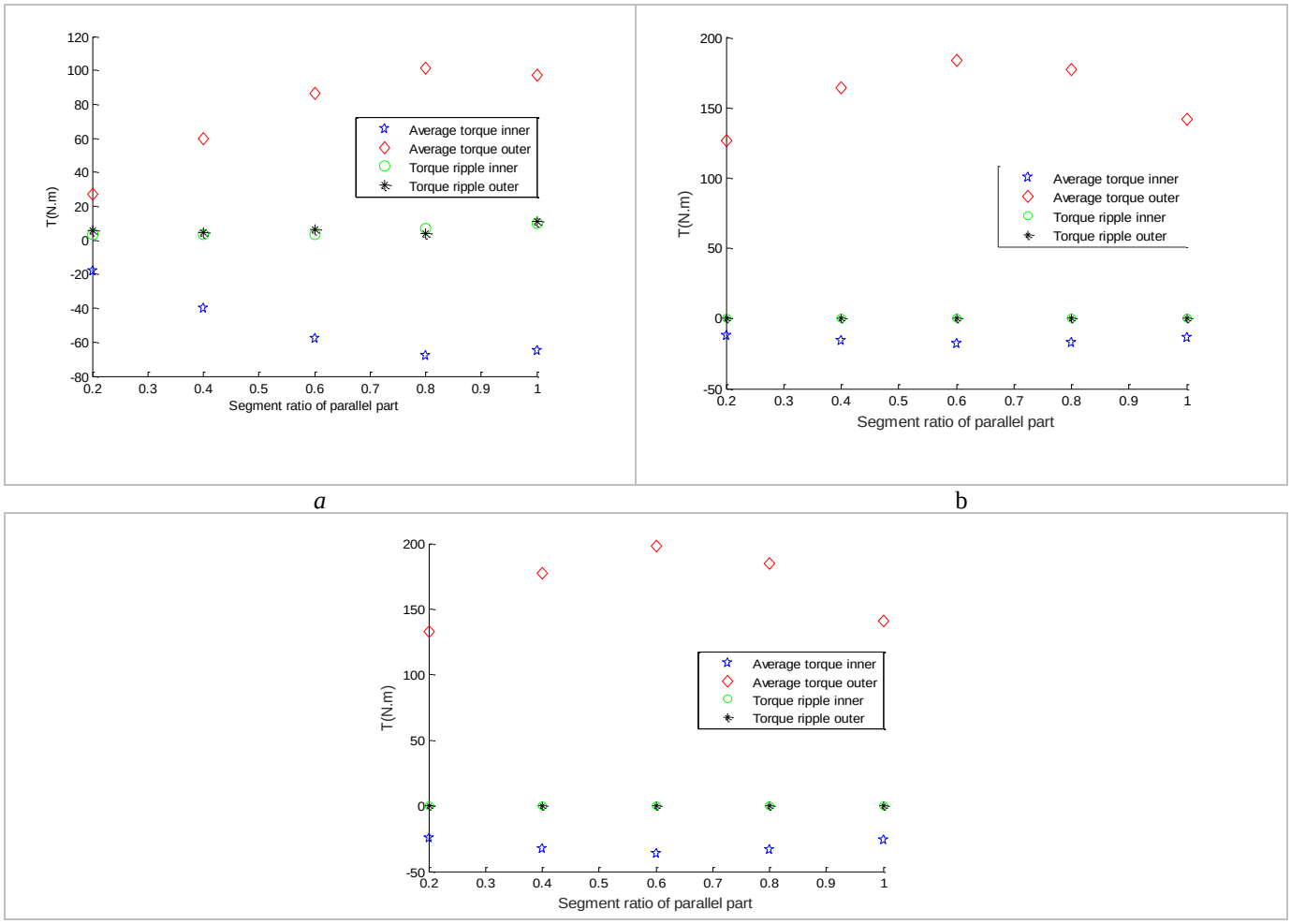

Fig. 6. *Transmitted torque and torque ripple for all cases with different segment ratios in two-segment magnetization pattern*

a Case 1 *(P_i=2, P_o=3)*
b Case 2 (P_i=2, P_o=21)
c Case 3 (P_i=4, P_o=22)

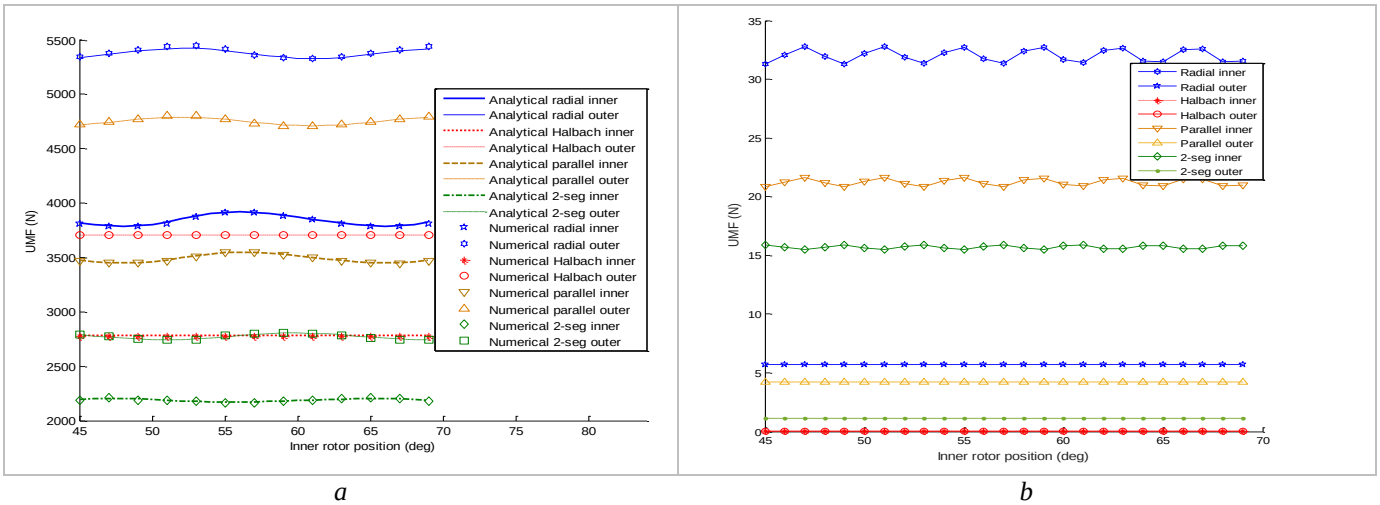

Fig. 7. *UMF of the two cases with different magnetization patterns*

a Case 1 *(P_i=2, P_o=3)*
b Case 2 (P_i=2, P_o=21)

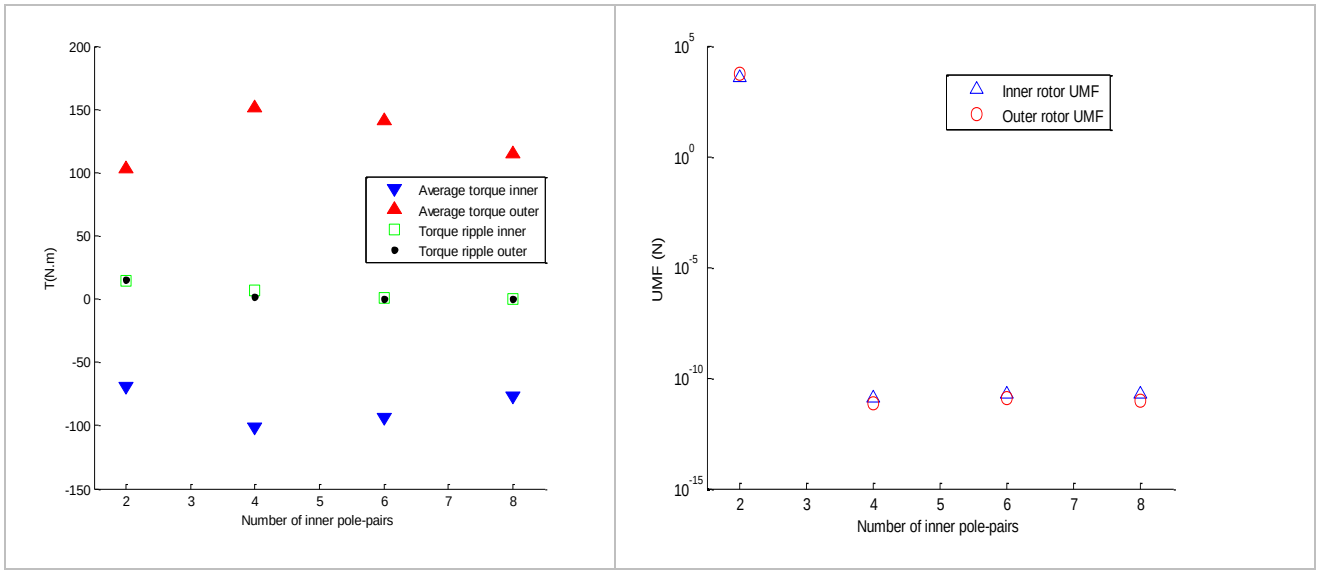

a *b*

Fig. 8. *Transmitted torque and torque ripple with different number of pole-pairs while the gear ratio is constant for radial magnetization pattern (Gr=1:1.5)*

a Torque vs. number of pole-pair
b UMF vs. number of pole-pair

4.6. Constant gear ratio with different number of pole-pieces

In this section, the influences of the number of pole-pieces for a constant gear ratio on the transmitted torque, torque ripple and UMF are investigated. To this end, four case studies all with gear ratio of 1:1.5 are considered which are P_i=2, P_o=3; P_i=4, P_o=6; P_i=6, P_o=9; and P_i=8, P_o=12.

The transmitted torque and the torque ripple of the inner and outer rotors versus the number of the inner pole-pairs is shown in Fig. 8.a. As evident, the maximum torque is transmitted in the case of P_i=4, P_o=6 and the torque ripple is low in the three last cases, because of high number of pole-pieces. Fig. 8.b shows the UMF versus the number of the inner pole-pairs. In contrast to the case of P_i=2, P_o=3, the other cases have low UMF, because of high number of pole-pieces. In this investigation the dimension of all the magnetic gears is identical to that listed in Table 2.

5. Discussion

The influences of different magnetization patterns on the performance of three magnetic gears have been investigated. The effects of the slot-opening ratio on three case studies each with different magnetization patterns have also been investigated. In the case of magnetic gears with two-segment Halbach magnetization pattern, the effects of the segment ratio on the transmitted torque and torque ripple have been

examined for three case studies. Table 8 compares the performance of the three magnetic gears in terms of average torque, torque ripple and UMF under different magnetization patterns.

The optimal slot-opening ratio to transmit maximum torque is highly dependent on the number of pole-pieces. When the number of pole-pieces is low, the maximum torque is transmitted if the slot-opening ratio is set to 0.3 regardless of the magnetization pattern. At higher number of pole-pieces, the maximum torque capability is achieved for the slot-opening ratio of 0.55.

In the case of two-segment magnetization pattern, the segment ratio affects the average torque and torque ripple. However, its optimum value depends on the number of pole-pieces. At low number of pole-pieces, the segment ratio of 0.8 results in maximum average torque and minimum torque ripple. As the number of pole-pieces increases, the segment ratio of 0.6 causes maximum average torque and minimum torque ripple.

For a given gear ratio and a predefined gear volume, there is a number of pole-pieces in which the performance of the magnetic gear, in terms of transmitted torque, torque ripple and UMF, is optimized.

Table 8 Effects of the magnetization patterns on the performance of magnetic gears

Cases	Quantity	Rank 1(Best)	Rank 2	Rank 3	Rank 4(worst)
1 P_i=2 P_o=3	Average torque	Radial	Parallel	Halbach	2-seg.
	Torque ripple	Halbach	Parallel	Radial	2-seg.
	UMF	2-seg.	Halbach	Parallel	Radial
2 P_i=2 P_o=21	Average torque	Halbach	2-seg.	Parallel	Radial
	Torque ripple	Almost zero			
	UMF	Halbach	2-seg.	Parallel	Radial
3 P_i=4 P_o=22	Average torque	Halbach	2-seg.	Parallel	Radial
	Torque ripple	Almost zero			
	UMF	Almost zero			

6. Conclusions

A 2-D analytical model for coaxial magnetic gears with different magnetization patterns, i.e. radial, parallel, ideal Halbach and two-segment Halbach, has been derived. The analytical results of the magnetic flux density, transmitted torque and unbalanced magnetic force have been compared with those of the numerical results to show the accuracy of the analytical model. In general, to improve the performance of a magnetic gear in terms of maximum transmitted torque, minimum torque ripple and minimum UMF, the type of magnetization pattern, the slot-opening ratio and the number of pole-pieces are among the crucial variables which should be optimally selected. In addition, for the case of multi-segment Halbach magnetization pattern, the ratio of each segment plays an important role in the performance of the magnetic gear. Although a magnetic gear with the ideal Halbach magnetization pattern outperforms its rivals with other magnetization patterns, due to the high manufacturing cost of the ideal Halbach, the two-segment

Halbach magnetization pattern can be an alternative if the performance and cost are both of prime importance. Finally, for a specified gear ratio and magnetic gear volume number of pole-pieces has a great influence on the performance of magnetic gears, i.e. transmitted torque, torque ripple and UMF.

7. Appendix A

The radial and tangential components of the four magnetization patterns are expressed as follows for both the inner and outer permanent magnets:

I) Ideal Halbach:
For inner PMs:

$$M_r^{im} = \frac{B_r}{\mu_0}\sin(P(\theta-\varphi)) \quad (58) \qquad M_\theta^{im} = \frac{B_r}{\mu_0}\cos(P(\theta-\varphi)) \quad (59)$$

For outer PMs:

$$M_r^{om} = \frac{B_r}{\mu_0}\sin(P(\theta-\varphi)) \quad (60) \qquad M_\theta^{om} = -\frac{B_r}{\mu_0}\cos(P(\theta-\varphi)) \quad (61)$$

II) Radial:
For both inner and outer PMs:

$$M_r^{i} = \begin{cases} \frac{B_r}{\mu_0} & \varphi+\gamma \le \theta \le \varphi+\gamma+\alpha\frac{\pi}{P} \\ 0 & otherwise \\ -\frac{B_r}{\mu_0} & \varphi-\gamma-\alpha\frac{\pi}{P} \le \theta \le \varphi-\gamma \end{cases} \quad (62) \qquad M_\theta^{i} = 0 \quad (63)$$

III) Two segment Halbach:
For inner PMs:

$$M_r^{im} = \begin{cases} \frac{-B_r}{\mu_0}\sin(\theta+(-\varphi+\frac{k_T\pi}{P}+\frac{k_R\pi}{P}+2\gamma)) & \varphi-\frac{k_T\pi}{P}-\frac{k_R\pi}{P}-2\gamma \le \theta \le \varphi-\frac{k_T\pi}{2P}-\frac{k_R\pi}{P}-2\gamma \\ \frac{-B_r}{\mu_0}\cos(\theta+(-\varphi+\frac{k_T\pi}{2P}+\frac{k_R\pi}{2P}+\gamma)) & \varphi-\frac{k_T\pi}{2P}-\frac{k_R\pi}{P}-\gamma \le \theta \le \varphi-\frac{k_T\pi}{2P}-2\gamma \\ \frac{B_r}{\mu_0}\sin(\theta-\varphi) & \varphi-\frac{k_T\pi}{2P} \le \theta \le \varphi+\frac{k_T\pi}{2P} \\ \frac{B_r}{\mu_0}\cos(\theta-(\varphi+\frac{k_T\pi}{2P}+\frac{k_R\pi}{2P}+\gamma)) & \varphi+\frac{k_T\pi}{2P}+\gamma \le \theta \le \varphi+\frac{k_T\pi}{2P}+\frac{k_R\pi}{P}+\gamma \\ \frac{-B_r}{\mu_0}\sin(\theta-(\varphi+\frac{k_T\pi}{P}+\frac{k_R\pi}{P}+2\gamma)) & \varphi+\frac{k_T\pi}{2P}+\frac{k_R\pi}{P}+2\gamma \le \theta \le \varphi+\frac{k_T\pi}{P}+\frac{k_R\pi}{P}+2\gamma \\ 0 & otherwise \end{cases} \quad (64)$$

$$M_\theta^{im} = \begin{cases} \frac{-B_r}{\mu_0}\cos(\theta+(-\varphi+\frac{k_T\pi}{P}+\frac{k_R\pi}{P}+2\gamma)) & \varphi-\frac{k_T\pi}{P}-\frac{k_R\pi}{P}-2\gamma \le \theta \le \varphi-\frac{k_T\pi}{2P}-\frac{k_R\pi}{P}-2\gamma \\ \frac{B_r}{\mu_0}\sin(\theta+(-\varphi+\frac{k_T\pi}{2P}+\frac{k_R\pi}{2P}+\gamma)) & \varphi-\frac{k_T\pi}{2P}-\frac{k_R\pi}{P}-\gamma \le \theta \le \varphi-\frac{k_T\pi}{2P}-2\gamma \\ \frac{B_r}{\mu_0}\cos(\theta-\varphi) & \varphi-\frac{k_T\pi}{2P} \le \theta \le \varphi+\frac{k_T\pi}{2P} \\ \frac{-B_r}{\mu_0}\sin(\theta-(\varphi+\frac{k_T\pi}{2P}+\frac{k_R\pi}{2P}+\gamma)) & \varphi+\frac{k_T\pi}{2P}+\gamma \le \theta \le \varphi+\frac{k_T\pi}{2P}+\frac{k_R\pi}{P}+\gamma \\ \frac{-B_r}{\mu_0}\cos(\theta-(\varphi+\frac{k_T\pi}{P}+\frac{k_R\pi}{P}+2\gamma)) & \varphi+\frac{k_T\pi}{2P}+\frac{k_R\pi}{P}+2\gamma \le \theta \le \varphi+\frac{k_T\pi}{P}+\frac{k_R\pi}{P}+2\gamma \\ 0 & otherwise \end{cases} \quad (65)$$

For outer PMs:

$$M_r^{om}=\begin{cases}\frac{B_r}{\mu_0}\sin(\theta+(-\varphi+\frac{k_T\pi}{P}+\frac{k_R\pi}{P}+2\gamma)) & \varphi-\frac{k_T\pi}{P}-\frac{k_R\pi}{P}-2\gamma\le\theta\le\varphi-\frac{k_T\pi}{2P}-\frac{k_R\pi}{P}-2\gamma\\ \frac{-B_r}{\mu_0}\cos(\theta+(-\varphi+\frac{k_T\pi}{2P}+\frac{k_R\pi}{2P}+\gamma)) & \varphi-\frac{k_T\pi}{2P}-\frac{k_R\pi}{P}-\gamma\le\theta\le\varphi-\frac{k_T\pi}{2P}-2\gamma\\ \frac{-B_r}{\mu_0}\sin(\theta-\varphi) & \varphi-\frac{k_T\pi}{2P}\le\theta\le\varphi+\frac{k_T\pi}{2P}\\ \frac{B_r}{\mu_0}\cos(\theta-(\varphi+\frac{k_T\pi}{2P}+\frac{k_R\pi}{2P}+\gamma)) & \varphi+\frac{k_T\pi}{2P}+\gamma\le\theta\le\varphi+\frac{k_T\pi}{2P}+\frac{k_R\pi}{P}+\gamma\\ \frac{B_r}{\mu_0}\sin(\theta-(\varphi+\frac{k_T\pi}{P}+\frac{k_R\pi}{P}+2\gamma)) & \varphi+\frac{k_T\pi}{2P}+\frac{k_R\pi}{P}+2\gamma\le\theta\le\varphi+\frac{k_T\pi}{P}+\frac{k_R\pi}{P}+2\gamma\\ 0 & otherwise\end{cases} \quad (66)$$

$$M_\theta^{om}=\begin{cases}\frac{B_r}{\mu_0}\cos(\theta+(-\varphi+\frac{k_T\pi}{P}+\frac{k_R\pi}{P}+2\gamma)) & \varphi-\frac{k_T\pi}{P}-\frac{k_R\pi}{P}-2\gamma\le\theta\le\varphi-\frac{k_T\pi}{2P}-\frac{k_R\pi}{P}-2\gamma\\ \frac{B_r}{\mu_0}\sin(\theta+(-\varphi+\frac{k_T\pi}{2P}+\frac{k_R\pi}{2P}+\gamma)) & \varphi-\frac{k_T\pi}{2P}-\frac{k_R\pi}{P}-\gamma\le\theta\le\varphi-\frac{k_T\pi}{2P}-2\gamma\\ \frac{-B_r}{\mu_0}\cos(\theta-\varphi) & \varphi-\frac{k_T\pi}{2P}\le\theta\le\varphi+\frac{k_T\pi}{2P}\\ \frac{-B_r}{\mu_0}\sin(\theta-(\varphi+\frac{k_T\pi}{2P}+\frac{k_R\pi}{2P}+\gamma)) & \varphi+\frac{k_T\pi}{2P}+\gamma\le\theta\le\varphi+\frac{k_T\pi}{2P}+\frac{k_R\pi}{P}+\gamma\\ \frac{B_r}{\mu_0}\cos(\theta-(\varphi+\frac{k_T\pi}{P}+\frac{k_R\pi}{P}+2\gamma)) & \varphi+\frac{k_T\pi}{2P}+\frac{k_R\pi}{P}+2\gamma\le\theta\le\varphi+\frac{k_T\pi}{P}+\frac{k_R\pi}{P}+2\gamma\\ 0 & otherwise\end{cases} \quad (67)$$

IV) Parallel:

The expression is similar to that of the two-segment Halbach, but $K_r=1$ and $K_t=0$.

Consider the following Fourier series expansions of the radial and tangential components of the magnetization vector for both the inner and outer PMs:

$$M_r^{im}=\sum_{h=1}^{N}\left(M_{rh}^{im}\cos(hP_{im}\theta)+N_{rh}^{im}\sin(hP_{im}\theta)\right) \quad (68)$$

$$N_\theta^{im}=\sum_{h=1}^{N}\left(M_{\theta h}^{im}\cos(hP_{im}\theta)+N_{\theta h}^{im}\sin(hP_{im}\theta)\right) \quad (69)$$

$$M_r^{om}=\sum_{h=1}^{N}\left(M_{rh}^{om}\cos(hP_{om}\theta)+N_{rh}^{om}\sin(hP_{om}\theta)\right) \quad (70)$$

$$N_\theta^{om}=\sum_{h=1}^{N}\left(M_{\theta h}^{om}\cos(hP_{om}\theta)+N_{\theta h}^{om}\sin(hP_{om}\theta)\right) \quad (71)$$

where M_{rh}^{im}, $N_{\theta h}^{im}$, M_{rh}^{om}, $N_{\theta h}^{om}$ are the Fourier series coefficients of the radial and tangential components of the magnetization vector which are different in each magnetization pattern. Substitution (32) into (14) yields the following relations for the inner and outer PMs respectively:

$$k_{n1}^{im}(r)=\begin{cases}\frac{-\mu_0\left(M_{\theta h}^{im}-hP_{im}N_{rh}^{im}\right)}{\left(1-n^2\right)}r & ,n=hP_{im}\ ,h=1,2,3,...\\ \frac{-\mu_0}{2}\left(M_{\theta 1}^{im}-N_{r1}^{im}\right)r\ln(r) & ,n=P_{im}=1\end{cases} \quad (72)$$

$$k_{n2}^{im}(r)=\begin{cases}\frac{-\mu_0\left(N_{\theta h}^{im}+hP_{im}M_{rh}^{im}\right)}{\left(1-n^2\right)}r & ,n=hP_{im}\ ,h=1,2,3,...\\ \frac{-\mu_0}{2}\left(N_{\theta 1}^{im}+M_{r1}^{im}\right)r\ln(r) & ,n=P_{im}=1\end{cases} \quad (73)$$

$$k_{n1}^{om}(r)=\begin{cases}\frac{-\mu_0\left(M_{\theta h}^{om}-hP_{om}N_{rh}^{om}\right)}{\left(1-n^2\right)}r & ,n=hP_{om}\ ,h=1,2,3,...\\ \frac{-\mu_0}{2}\left(M_{\theta 1}^{om}-N_{r1}^{om}\right)r\ln(r) & ,n=P_{om}=1\end{cases} \quad (74)$$

$$k_{n2}^{om}(r)=\begin{cases}\frac{-\mu_0\left(N_{\theta n}^{om}+hP_{om}M_{rn}^{om}\right)}{\left(1-n^2\right)}r & ,n=hP_{om}\ ,h=1,2,3,...\\ \frac{-\mu_0}{2}\left(N_{\theta 1}^{om}+M_{r1}^{om}\right)r\ln(r) & ,n=P_{om}=1\end{cases} \quad (75)$$

Imposing the boundary/interface conditions (20)-(30) yields the following algebraic simultaneous equations in which the integral coefficients are unknowns. According to (20) the following expressions are obtained:

$$\hat{a}_n^{im} n\left(\frac{R_{im}}{R_{ia}}\right)^n - \hat{b}_n^{im} n + R_{im}\left.\frac{d(k_{n1}^{im})}{dr}\right|_{r=R_{im}} + R_{im}\mu_0 M_{\theta h}^{im} = 0 \quad (76)$$

$$\hat{c}_n^{im} n\left(\frac{R_{im}}{R_{ia}}\right)^n - \hat{d}_n^{im} n + R_{im}\left.\frac{d(k_{n2}^{im})}{dr}\right|_{r=R_{im}} + R_{im}\mu_0 N_{\theta h}^{im} = 0 \quad (77)$$

where $\hat{a}_n^{im}, \hat{b}_n^{im}, \hat{c}_n^{im}, \hat{d}_n^{im}$ are the integral coefficients, $\left.\frac{d(k_{n1}^{im})}{dr}\right|_{r=R_{im}}$ and $\left.\frac{d(k_{n2}^{im})}{dr}\right|_{r=R_{im}}$ are the derivative of the particular solutions with respect to *r* and $M_{\theta n}^{im}$ and $N_{\theta n}^{im}$ are the Fourier series coefficients of the tangential component of the inner PM magnetization vector. Applying (21) yields:

$$\hat{a}_n^{im} + \hat{b}_n^{im}\left(\frac{R_{im}}{R_{ia}}\right)^n + k_{n1}^{im}\Big|_{r=R_{ia}} = \hat{a}_n^{ia}\left(\frac{R_{ia}}{R_{is}}\right)^n + \hat{b}_n^{ia} \quad (78)$$

$$\hat{c}_n^{im} + \hat{d}_n^{im}\left(\frac{R_{im}}{R_{ia}}\right)^n + k_{n2}^{i}\Big|_{r=R_{ia}} = \hat{c}_n^{ia}\left(\frac{R_{ia}}{R_{is}}\right)^n + \hat{d}_n^{ia} \quad (79)$$

According to (22), the following relations are obtained:

$$\hat{a}_n^{ia} n\left(\frac{R_{ia}}{R_{is}}\right)^n - n\hat{b}_n^{ia} = \frac{1}{\mu_r}\left(\hat{a}_n^{im} n - \hat{b}_n^{im} n\left(\frac{R_{im}}{R_{ia}}\right)^n + R_{ia}\left.\frac{d(k_{n1}^{im})}{dr}\right|_{r=R_{ia}} + R_{ia}\mu_0 M_{\theta h}^{im}\right) \quad (80)$$

$$c_n^{ia} n\left(\frac{R_{ia}}{R_{is}}\right)^n - d_n^{ia} n = \frac{1}{\mu_r}\left(c_n^{im} n - d_n^{im} n\left(\frac{R_{im}}{R_{ia}}\right)^n + R_{ia}\left.\frac{d(k_{n2}^{im})}{dr}\right|_{r=R_{ia}} + R_{ia}\mu_0 N_{\theta h}^{im}\right) \quad (81)$$

According to equation (23)

$$a_0^{sl,j} + b_0^{sl,j}\ln(R_{is}) = a_0^{ia} + \sum_{n=1}^{N}\left(\hat{a}_n^{ia} + \hat{b}_n^{ia}\left(\frac{R_{is}}{R_{ia}}\right)^{-n}\right)\frac{1}{n\beta}\left(\sin(n(\theta_j+\beta) - \sin(n\theta_j)\right) + \sum_{n=1}^{N}\left(\hat{c}_n^{ia} + \hat{d}_n^{ia}\left(\frac{R_{is}}{R_{ia}}\right)^{-n}\right)\frac{1}{n\beta}\left(-\cos(n(\theta_j+\beta) + \cos(n\theta_j)\right) \quad (82)$$

$$\hat{a}_u^{sl,j} + \hat{b}_u^{sl,j}\left(\frac{R_{is}}{R_{os}}\right)^{\frac{u\pi}{\beta}} =$$
$$\sum_{n=1}^{N}\left(\hat{a}_n^{ia}\frac{1}{\beta} + \hat{b}_n^{ia}\frac{1}{\beta}\left(\frac{R_{is}}{R_{ia}}\right)^{-n}\right)\times$$
$$\left(\begin{array}{l}\frac{1}{(n+\frac{u\pi}{\beta})}\left[\sin(n\theta_j + n\beta + u\pi) - \sin(n\theta_j)\right] + \\ \frac{1}{(n-\frac{u\pi}{\beta})}\left[\sin(n\theta_j + n\beta - u\pi) - \sin(n\theta_j)\right]\end{array}\right) +$$
$$\sum_{n=1}^{N}\left(\hat{c}_n^{ia}\frac{1}{\beta} + \hat{d}_n^{ia}\frac{1}{\beta}\left(\frac{R_{is}}{R_{ia}}\right)^{-n}\right)\times \qquad (83)$$
$$\left(\begin{array}{l}\frac{1}{(n+\frac{u\pi}{\beta})}\left[-\cos(n\theta_j + n\beta + u\pi) + \cos(n\theta_j)\right] + \\ \frac{1}{(n-\frac{u\pi}{\beta})}\left[-\cos(n\theta_j + n\beta - u\pi) + \cos(n\theta_j)\right]\end{array}\right)$$

for $n \neq u\pi/\beta$

$$\hat{a}_u^{sl,j} + \hat{b}_u^{sl,j}\left(\frac{R_{is}}{R_{os}}\right)^{\frac{u\pi}{\beta}} =$$
$$\sum_{n=1}^{N}\left(\hat{a}_n^{ia} + \hat{b}_n^{ia}\left(\frac{R_{is}}{R_{ia}}\right)^{-n}\right)\times$$
$$\frac{1}{2n\beta}\left(\begin{array}{l}\left[2n\beta + \sin(2n(\theta_j + \beta) - \sin(2n\theta_j)\right]\cos\left(\frac{u\pi}{\beta}\theta_j\right) + \\ \left[-\cos(2n(\theta_j + \beta)) + \cos(2n\theta_j)\right]\sin\left(\frac{u\pi}{\beta}\theta_j\right)\end{array}\right) +$$
$$\sum_{n=1}^{N}\left(\hat{c}_n^{ia} + \hat{d}_n^{ia}\left(\frac{R_{is}}{R_{ia}}\right)^{-n}\right)\times \qquad (84)$$
$$\frac{1}{2n\beta}\left(\begin{array}{l}\left[-\cos(2n(\theta_j + \beta) + \cos(2n\theta_j)\right]\cos\left(\frac{u\pi}{\beta}\theta_j\right) + \\ \left[2n\beta - \sin(2n(\theta_j + \beta)) + \sin(2n\theta_j)\right]\sin\left(\frac{u\pi}{\beta}\theta_j\right)\end{array}\right)$$

for $n = u\pi/\beta$

According to (24):

$$\hat{a}_n^{ia} n - \hat{b}_n^{ia} n \left(\frac{R_{is}}{R_{ia}}\right)^{-n} =$$
$$\sum_{j=1}^{Q} \frac{b_0^j}{n\pi}\left(\sin(n(\theta_j + \beta)) - \sin(n\theta_j)\right) +$$
$$\sum_{j=1}^{Q}\sum_{u=1}^{U}\left(\hat{a}_u^{sl,j}\,\frac{-u}{\beta} + \hat{b}_u^{sl,j}\,\frac{u}{\beta}\left(\frac{R_{is}}{R_{os}}\right)^{\frac{u\pi}{\beta}}\right)\times \qquad (85)$$
$$\begin{pmatrix} \frac{1}{2(\frac{u\pi}{\beta}+n)}\left[\sin(u\pi + n\theta_j + n\beta) - \sin(n\theta_j)\right] + \\ \frac{1}{2(\frac{u\pi}{\beta}-n)}\left[\sin(u\pi - n\theta_j - n\beta) - \sin(-n\theta_j)\right] \end{pmatrix}$$

for $n \neq u\pi/\beta$

$$\hat{a}_n^{ia} n - \hat{b}_n^{ia} n \left(\frac{R_{is}}{R_{ia}}\right)^{-n} =$$
$$\sum_{i=1}^{Q} \frac{b_0^i}{n\pi}\left[\sin(n(\theta_j + \beta)) - \sin(n\theta_j)\right] +$$
$$\sum_{j=1}^{Q}\sum_{u=1}^{U}\left(\hat{a}_u^{sl,j}\,\frac{-u}{\beta} + \hat{b}_u^{sl,j}\,\frac{u}{\beta}\left(\frac{R_{is}}{R_{os}}\right)^{\frac{u\pi}{\beta}}\right)\times \qquad (86)$$
$$\begin{pmatrix} \frac{\cos(n\theta_j)}{4n}\left[2n\beta + \sin(2n(\theta_j + \beta)) - \sin(2n\theta_j)\right] + \\ \frac{\sin(n\theta_j)}{4n}\left[-\cos(2n(\theta_j + \beta)) + \cos(2n\theta_j)\right] \end{pmatrix}$$

for $n = u\pi/\beta$

$$\hat{c}_n^{ia} n - \hat{d}_n^{ia} n \left(\frac{R_{is}}{R_{ia}}\right)^{-n} =$$
$$\sum_{j=1}^{Q} \frac{b_0^i}{n\pi}\left(-\cos(n(\theta_j + \beta)) + \cos(n\theta_j)\right) +$$
$$\sum_{j=1}^{Q}\sum_{u=1}^{U}\left(\hat{a}_u^{sl,j}\,\frac{-u}{\beta} + \hat{b}_u^{sl,j}\,\frac{u}{\beta}\left(\frac{R_{is}}{R_{os}}\right)^{\frac{u\pi}{\beta}}\right)\times \qquad (87)$$
$$\begin{pmatrix} \frac{1}{2(n+\frac{u\pi}{\beta})}\left[-\cos(u\pi + n\theta_j + n\beta)\cos(n\theta_j)\right] + \\ \frac{1}{2(n-\frac{u\pi}{\beta})}\left[-\cos(-u\pi + n\theta_j + n\beta) + \cos(n\theta_j)\right] \end{pmatrix}$$

for $n \neq u\pi/\beta$

$$\hat{c}_n^{ia} n - \hat{d}_n^{ia} n \left(\frac{R_{is}}{R_{ia}}\right)^{-n} =$$

$$\sum_{j=1}^{Q} \frac{b_0^j}{n\pi}\left[-\cos(n(\theta_j+\beta))+\cos(n\theta_j)\right]+$$

$$\sum_{j=1}^{Q}\sum_{u=1}^{U}\left(\hat{a}_u^j \frac{-u}{\beta} + \hat{b_u^j}\frac{u}{\beta}\left(\frac{R_{is}}{R_{os}}\right)^{\frac{u\pi}{\beta}}\right)\times \qquad (88)$$

$$\begin{pmatrix} \frac{\cos(n\theta_j)}{4n}\left[-\cos(2n(\theta_j+\beta))+\cos(2n\theta_j)\right]+ \\ \frac{\sin(n\theta_j)}{4n}\left[2n\beta-\sin(2n(\theta_j+\beta))+\sin(2n\theta_j)\right] \end{pmatrix},$$

for $n=u\pi/\beta$

According to (25):

$$a_0^{sl,j} + b_0^{sl,j}\ln(R_{os}) =$$

$$\sum_{n=1}^{N}\left(\hat{a}_n^{oa}\left(\frac{R_{os}}{R_{oa}}\right)^n + \hat{b}_n^{oa}\right)\frac{1}{n\beta}\left(\sin(n(\theta_j+\beta)-\sin(n\theta_j)\right)+ \qquad (89)$$

$$\sum_{n=1}^{N}\left(\hat{c}_n^{oa}\left(\frac{R_{os}}{R_{oa}}\right)^n + \hat{d}_n^{oa}\right)\frac{1}{n\beta}\left(-\cos(n(\theta_j+\beta))+\cos(n\theta_j)\right)$$

$$\hat{a}_u^{sl,j}\left(\frac{R_{os}}{R_{is}}\right)^{-\frac{u\pi}{\beta}} + \hat{b}_u^{sl,j} =$$

$$\sum_{n=1}^{N}\left(\hat{a}_n^{oa}\left(\frac{R_{os}}{R_{oa}}\right)^n + \hat{b}_n^{oa}\right)\times$$

$$\begin{pmatrix} \frac{1}{(n\beta+u\pi)}\left[\sin(n\theta_j+n\beta+u\pi)-\sin(n\theta_j)\right]+ \\ \frac{1}{2(n\beta-u\pi)}\left[\sin(n\theta_j+n\beta-u\pi)-\sin(n\theta_j)\right] \end{pmatrix}+$$

$$\sum_{n=1}^{N}\left(\hat{c}_n^{oa}\left(\frac{R_{os}}{R_{oa}}\right)^n + \hat{d}_n^{oa}\right)\times \qquad (90)$$

$$\begin{pmatrix} \frac{1}{(n\beta+u\pi)}\left[-\cos(n\theta_j+n\beta+u\pi)+\cos(n\theta_j)\right]+ \\ \frac{1}{(n\beta-u\pi)}\left[-\cos(n\theta_j+n\beta-u\pi)+\cos(n\theta_j)\right] \end{pmatrix}$$

for $n\neq u\pi/\beta$

$$\hat{a}_u^{sl,j}\left(\frac{R_{os}}{R_{is}}\right)^{-\frac{u\pi}{\beta}}+\hat{b}_u^{sl,j}=$$
$$\sum_{n=1}^{N}\left(\hat{a}_n^{oa}\left(\frac{R_{os}}{R_{oa}}\right)^{n}+\hat{b}_n^{oa}\right)\times$$
$$\frac{1}{2n\beta}\left(\begin{array}{l}\left[2n\beta+\sin(2n(\theta_j+\beta))-\sin(2n\theta_j)\right]\cos\left(n\theta_j\right)+\\ \left[-\cos(2n(\theta_j+\beta))+\cos(2n\theta_j)\right]\sin\left(n\theta_j\right)\end{array}\right)+$$
$$\sum_{n=1}^{N}\left(\hat{c}_n^{oa}\left(\frac{R_{os}}{R_{oa}}\right)^{n}+\hat{d}_n^{oa}\right)\times \qquad (91)$$
$$\frac{1}{2n\beta}\left(\begin{array}{l}\left[-\cos(2n(\theta_j+\beta))+\cos(2n\theta_j)\right]\cos\left(n\theta_j\right)+\\ \left[2n\beta-\sin(2n(\theta_j+\beta))+\sin(2n\theta_j)\right]\sin\left(n\theta_j\right)\end{array}\right)$$

for $n=u\pi/\beta$

According to (26):

$$\hat{a}_n^{oa}n\left(\frac{R_{os}}{R_{oa}}\right)^{n}-\hat{b}_n^{oa}n=$$
$$\sum_{j=1}^{Q}\frac{b_0^j}{n\pi}\left(\sin(n(\theta_j+\beta))-\sin(n\theta_j)\right)+$$
$$\sum_{j=1}^{Q}\sum_{u=1}^{U}\left(\hat{a}_u^{sl,j}\frac{-u}{\beta}\left(\frac{R_{os}}{R_{is}}\right)^{-\frac{u\pi}{\beta}}+\hat{b}_u^{sl,j}\frac{u}{\beta}\right)\times$$
$$\left(\begin{array}{l}\frac{1}{2(n+\frac{u\pi}{\beta})}\left[\sin(u\pi+n\theta_j+n\beta)-\sin(n\theta_j)\right]+\\ \frac{1}{2(n-\frac{u\pi}{\beta})}\left[\sin(n\theta_j+n\beta-u\pi)-\sin(n\theta_j)\right]\end{array}\right) \qquad (92)$$

for $n\neq u\pi/\beta$

$$\hat{a}_n^{oa}n\left(\frac{R_{os}}{R_{oa}}\right)^{n}-\hat{b}_n^{oa}n=$$
$$\sum_{j=1}^{Q}\frac{b_0^{sl,j}}{n\pi}\left(\sin(n(\theta_j+\beta))-\sin(n\theta_j)\right)+$$
$$\sum_{j=1}^{Q}\sum_{u=1}^{U}\left(\hat{a}_u^{sl,j}\frac{-u}{\beta}\left(\frac{R_{os}}{R_{is}}\right)^{-\frac{u\pi}{\beta}}+\hat{b}_u^{sl,j}\frac{u}{\beta}\right)\times \qquad (93)$$
$$\frac{1}{4n}\left(\begin{array}{l}\left[2n\beta+\sin(2n(\theta_j+\beta))-\sin(2n\theta_j)\right]\cos(\mathrm{n}\,\theta_j)+\\ \left[-\cos(2n(\theta_j+\beta))+\cos(2n\theta_j)\right]\sin(n\theta_j)\end{array}\right)$$

for $n=u\pi/\beta$

$$\hat{c}_n^{oa} n \left(\frac{R_{os}}{R_{oa}}\right)^n - \hat{d}_n^{oa} n =$$

$$\sum_{j=1}^{Q} \frac{b_0^j}{n\pi}\left(-\cos(n(\theta_j+\beta)) + \cos(n\theta_j)\right) +$$

$$\sum_{j=1}^{Q}\sum_{u=1}^{U}\left(\hat{a}_u^{sl,j}\frac{-u}{\beta}\left(\frac{R_{os}}{R_{is}}\right)^{-\frac{u\pi}{\beta}} + \hat{b}_u^{sl,j}\frac{u}{\beta}\right)\times$$

$$\left(\begin{array}{l}\dfrac{1}{2(n+\frac{u\pi}{\beta})}\left[-\cos(u\pi + n\theta_j + n\beta) + \cos(n\theta_j)\right] + \\ \dfrac{1}{2(n-\frac{u\pi}{\beta})}\left[-\cos(-u\pi + n\theta_j + n\beta) + \cos(n\theta_j)\right]\end{array}\right) \qquad (94)$$

for $n \neq u\pi/\beta$

$$\hat{c}_n^{oa} n \left(\frac{R_{os}}{R_{oa}}\right)^n - \hat{d}_n^{oa} n =$$

$$\sum_{j=1}^{Q} \frac{b_0^{sl,j}}{n\pi}\left(-\cos(\mathrm{n}(\theta_j+\beta)) + \cos(n\theta_j)\right) +$$

$$\sum_{j=1}^{Q}\sum_{u=1}^{U}\left(\hat{a}_u^{sl,j}\frac{-u}{\beta}\left(\frac{R_{os}}{R_{is}}\right)^{-\frac{u\pi}{\beta}} + \hat{b}_u^{sl,j}\frac{u}{\beta}\right)\times \qquad (95)$$

$$\frac{1}{4n}\left(\begin{array}{l}\left[-\cos(2n(\theta_j+\beta)) + \cos(2n\theta_j)\right]\cos(\mathrm{n}\theta_j) + \\ \left[2n\beta - \sin(2n(\theta_j+\beta)) + \sin(2n\theta_j)\right]\sin(n\theta_j)\end{array}\right)$$

for $n = u\pi/\beta$

According to (27):

$$\hat{a}_n^{om}\left(\frac{R_{oa}}{R_{om}}\right)^n + \hat{b}_n^{om} + K_{n1}^{om}\Big|_{r=R_{oa}} = \hat{a}_n^{oa} + \hat{b}_n^{oa}\left(\frac{R_{oa}}{R_{os}}\right)^{-n} \qquad (96)$$

$$\hat{c}_n^{om}\left(\frac{R_{oa}}{R_{om}}\right)^n + \hat{d}_n^{om} + K_{n2}^{om}\Big|_{r=R_{oa}} = \hat{c}_n^{oa} + \hat{d}_n^{oa}\left(\frac{R_{oa}}{R_{os}}\right)^{-n} \qquad (97)$$

According to (28):

$$\hat{a}_n^{oa} n - \hat{b}_n^{oa} n\left(\frac{R_{oa}}{R_{os}}\right)^{-n} =$$

$$\frac{1}{\mu_r}\left(\hat{a}_n^{om} n\left(\frac{R_{oa}}{R_{om}}\right)^n - \hat{b}_n^{om} n + R_{oa}\frac{d(K_{n1}^{om})}{dr}\Big|_{r=R_{oa}} + R_{oa}\mu_0 M_{\theta h}^{om}\right) \qquad (98)$$

$$\hat{c}_n^{oa} n - \hat{d}_n^{oa} n\left(\frac{R_{oa}}{R_{os}}\right)^{-n} =$$

$$\frac{1}{\mu_r}\left(\hat{c}_n^{om} n\left(\frac{R_{oa}}{R_{om}}\right)^n - \hat{d}_n^{om} n + R_{oa}\frac{d(K_{n2}^{om})}{dr}\Big|_{r=R_{oa}} + R_{oa}\mu_0 N_{\theta h}^{om}\right) \qquad (99)$$

According to (29):

$$\hat{a}_n^{om} n - \hat{b}_n^{om} n \left(\frac{R_{om}}{R_{oa}}\right)^{-n} + R_{om} \left.\frac{d(K_{n1}^{om})}{dr}\right|_{r=R_{om}} + R_{om}\mu_0 M_{\theta h}^{om} = 0 \quad (100)$$

$$\hat{c}_n^{om} n - \hat{d}_n^{om} n \left(\frac{R_{om}}{R_{oa}}\right)^{-n} + R_{om} \left.\frac{d(K_{n2}^{om})}{dr}\right|_{r=R_{om}} + R_{om}\mu_0 N_{\theta h}^{om} = 0 \quad (101)$$

According to (30):

$$\sum_{j=1}^{Q} b_0^{sl,j} = 0 \quad (102)$$

8. References

[1] Atallah, K., Rens, J., Mezani, S., Howe, D.: 'A Novel Pseudo Direct-Drive Brushless Permanent Magnet Machine,' *IEEE Transactions on Magnetics*, Vol. 44, No. 11, pp. 4349-4352, November, 2008.

[2] Sun, X., Cheng, M., W. Hua, L. Xu, 'Optimal Design of Double-Layer Permanent Magnet Dual Mechanical Port Machine for Wind Power Application,' *IEEE Transactions on Magnetics*, Vol. 45, No. 10, pp. 4613-4616, October 2009.

[3] Wang, J., Atallah, K., Carvley, S.D., 'A Magnetic Continuously Variable Transmission Device' *IEEE Transactions on Magnetics*, Vol. 47, No. 10, pp. 2815-2818, October, 2011.

[4] Tsuruinoto, K., Kikuchi, S.: 'A New Magnetic Gear Using Permanent-Magnet,' *IEEE Transactions on Magnetics*, Vol. 23, No. 5, pp. 3622-3624, and September 1987.

[5] Yao, Y. D., Huang, D. R., Hsieh, C. C., Chian, D. Y. , Wang ,S. J.: 'Simulation Study of the Magnetic Coupling between Radial Magnetic Gears,' *IEEE Transactions on Magnetics*, Vol. 33, No. 2, pp. 2203-2206, March 1997.

[6] Yao,Y. D., Huang, D. R., Hsieh, C. C., Chiang, D. Y., Wang, S. J., Ying, T. F.: 'The Radial Magnetic Coupling Studies of Perpendicular Magnetic Gears,' *IEEE Transactions on Magnetics*, Vol. 32, No. 5, pp. 5061-5063, September 1996.

[7] Furlani, E. P.: 'A Two-Dimensional Analysis for the Coupling of Magnetic Gears,' *IEEE Transactions on Magnetics*, Vol. 33, No. 3, pp. 2317-2321, May 1997.

[8] Atallah, K., Howe, D.: 'A Novel High Performance Magnetic Gear,' *IEEE Transactions on Magnetics*, Vol. 37, No. 4, pp. 2844-2846, July 2001.
Okano, M., Tsurumoto, K., Togo, S., Tamada ,N., Fuchino, S., 'Characteristics of the Magnetic Gear using a Bulk High-Tc Superconductor,' *IEEE Transactions on Applied superconductivity*, Vol. 12, No. 1, pp. 979-983, March 2002.

[9] Atallah ,K., Calverley ,S.D., Howe D.: 'Design, Analysis and realization of a High-Performance Magnetic Gear,' *IEE Proc.-Electr. Power Appl.*, Vol. 151, No. 2, pp. 135-143, March 2004.

[10] Rasmussen, P.O., Andersen, T.O., Jørgensen, F.T., Nielsen, O.: 'Development of a High-Performance Magnetic Gear,' *IEEE Transactions on Industry Applications*, Vol. 41, No. 3, pp. 764-770, May/June 2005.

[11] Lubin, T., Mezani , S., Rezzoug, A.: 'Analytical Computation of the Magnetic Field Distribution in a Magnetic Gear,' *IEEE Transactions on Magnetics*, Vol. 46, No. 7, pp. 2611-2621, July 2010.

[12] Jian, L., Chau, K. T.: 'A Coaxial Magnetic Gear with Halbach Permanent-Magnet Arrays,' *IEEE Transactions on Energy Conversion*, Vol. 25, No. 2, pp. 319-328, June 2010.

[13] Shah, L., Cruden, A., Williams, B.W.: 'A Variable Speed Magnetic Gear Box Using Contra-Rotating Input Shafts,' *IEEE Transactions on Magnetics*, Vol. 47, No. 2, pp. 431-438, February 2011.

[14] Jing, L., Liu, L., Xiong, M., Feng, D.: 'Parameters Analysis and Optimization Design for a Concentric Magnetic Gear Based on Sinusoidal Magnetizations,' *IEEE Transactions on Applied superconductivity*, Vol. 24, No. 5, 0600905, October 2014.

[15] Mu Chen, Kwok Tong Chau Chunhua Liu 'Design of a new non-rare-earth magnetic variable gear for hybrid vehicular propulsion system' *IET Electr. Syst. Transp*., Vol. 3, pp. 57–66, 2013.

[16] Rahideh, A., Korakianitis, T.: 'Analytical magnetic field distribution of slotless brushless PM motors- Part I: Armature reaction field, inductance and rotor eddy current loss calculations,' *IET Electric Power Applications*, Vol. 6, No. 9, pp. 628-638, 2012 .

[17] Rahideh, A., Korakianitis, T.: 'Analytical magnetic field distribution of slotless brushless PM motors- Part II: Open-circuit field and torque calculations,' *IET Electric Power Applications*, Vol. 6, No. 9, pp. 639-651, 2012 .

[18] Rahideh, A., Mardaneh, M., Korakianitis, T.; 'Analytical 2D Calculations of Torque, Inductance and Back-EMF for Brushless Slotless Machines with Surface Inset Magnets,' *IEEE Transactions on Magnetics*, Vol. 49, No. 8, pp. 4873-4884, 2013 .

[19] Rahideh, A., Korakianitis, T.: 'Analytical Magnetic Field Calculation of Slotted brushless PM Machines With Surface Inset Magnets,' *IEEE Transactions on Magnetics*, Vol. 48, No. 10, pp. 2633-2649, Oct. 2012.

[20] Teymoori, S., Rahideh, A., Moayed-Jahromi, H., Mardaneh, M.: '2-D Analytical Magnetic Field Prediction for Consequent-Pole Permanent Magnet Synchronous Machines,' *IEEE Transactions on Magnetics*, Vol. 52, No.6, Article No.8202114, 2016.

[21] Moayed-Jahromi, H., Rahideh, A., Mardaneh, M.: '2-D Analytical Model for External Rotor Brushless PM Machines,' *IEEE Transactions on Energy Conversion*, Vol. 31, No. 3, pp. 1100-1109, Sep. 2016.

[22] Shenzi, Y., Zhu, Q.: 'General analytical model for calculating electromagnetic performance of permanent magnet brushless machines having segmented Halbach array' *IET Electr. Syst. Transp*., Vol. 6, pp. 153–162, 2016.

[23] Zarko, D., Ban, D., A. Lipo, T.: 'Analytical Solution for Cogging Torque in Surface Permanent-Magnet Motors Using Conformal Mapping' *IEEE Transactions on Magnetics*, Vol. 44, No. 1, pp. 52-65, 2008.